
Accelerating Safe Reinforcement Learning with Constraint-mismatched Policies

Tsung-Yen Yang
Princeton University
ty3@princeton.edu

Justinian Rosca
Siemens Corporation, Corporate Technology
justinian.rosca@siemens.com

Karthik Narasimhan
Princeton University
karthikn@cs.princeton.edu

Peter J. Ramadge
Princeton University
ramadge@princeton.edu

Abstract

We consider the problem of reinforcement learning when provided with a baseline control policy and a set of constraints that the controlled system must satisfy. The baseline policy might arise from a heuristic, a prior application, a teacher or demonstrator data. The constraints might encode safety, fairness or some application-specific requirements. We want to efficiently use reinforcement learning to adapt the baseline policy to improve performance and satisfy the given constraints when it is applied to the new system. The key challenge is to effectively use the baseline policy (which need not satisfy the current constraints) to aid the learning of a constraint-satisfying policy in the new application. We propose an iterative algorithm for solving this problem. Each iteration is composed of three-steps. The first step performs a policy update to increase the expected reward, the second step performs a projection to minimize the distance between the current policy and the baseline policy, and the last step performs a projection onto the set of policies that satisfy the constraints. This procedure allows the learning process to leverage the baseline policy to achieve faster learning while improving reward performance and satisfying the constraints imposed on the current problem. We analyze the convergence of the proposed algorithm and provide a finite-sample guarantee. Empirical results demonstrate that the algorithm can achieve superior performance, with 10 times fewer constraint violations and around 40% higher reward compared to state-of-the-art methods.

1 Introduction

Deep reinforcement learning (RL) has achieved superior performance in several domains such as games [1] and robotic control [2]. However, in these complex applications learning policies from scratch often requires tremendous resources (*e.g.*, time, energy). To resolve this issue, one would like to leverage a baseline policy available from a previous application or a teacher. The baseline policy may be sub-optimal for the new application and is not guaranteed to produce actions that satisfy given constraints on safety, fairness, or other costs. For instance, when you drive an unfamiliar vehicle, you do so cautiously to ensure safety, while at the same time you adapt your driving technique to the vehicle characteristics to improve your ‘driving reward’. In effect, you (as the agent) gradually adapt a baseline policy (*i.e.*, prior driving skill) to avoid violating the constraints (*e.g.*, safety) while improving your driving reward (*e.g.*, travel time, fuel efficiency).

This problem is challenging since directly leveraging the baseline policy, as in DAGGER [3] or GAIL [4], may result in policies that violate the constraints. To ensure constraint satisfaction in the new application, prior work either: adds a hyper-parameter weighted copy of the imitation learning

objective (*i.e.*, imitating the baseline policy) to the RL objective [5–7]; or pre-trains a policy with the baseline policy and fine-tunes it through RL [8, 9]. These approaches incur the cost of weight tuning and do not ensure constraint satisfaction on every learning episode.

In this work, to learn from the baseline policy, we propose an iterative algorithm that performs policy updates in three stages. The first step improves reward using a trust region policy optimization approach (*e.g.*, TRPO [10]). This can result in a new intermediate policy that is too far from the baseline policy and does not satisfy the constraints. The second step leverages the baseline policy by performing a projection to control the distance between the current policy and the baseline policy. This distance is updated depending on the reward improvement and constraint satisfaction on the current learning episode. This update method allows the learning algorithm to explore without being overly restricted by the (potentially constraint-violating) baseline policy [5], but still allows the baseline policy to influence the learning and does so without the computational burden of learning the cost function of the baseline policy [11]. The third step ensures constraint satisfaction by performing a projection onto the set of policies that satisfy the given constraints. This eliminates the issue of inefficient recovery from infeasible (*i.e.*, constraint-violating) states (*e.g.*, due to approximation errors), and tuning a weight of cost objective function added to the RL objective function [12]. We call the above algorithm *Safe Policy Adaptation with Constrained Exploration* (SPACE).

The paper’s contributions are as follows. We first analyze the convergence of SPACE and provide a finite-sample guarantee. We also provide an analysis of controlling the distance between the learned policy at iteration k and the baseline policy to ensure both feasibility of the optimization problem and exploration by the learning agent. We then empirically compare SPACE with state-of-the-art algorithms on three sets of control tasks, including two Mujoco environments with safety constraints from [13], two challenging traffic management tasks with fairness constraints from [14], and one human demonstration driving task with safety constraints from [15]. In all cases, SPACE achieves superior performance to prior approaches, averaging 40% more reward with 10 times fewer cost constraint violations. This shows that SPACE robustly learns constraint-satisfying policies, and serves as a step towards safe deployment of RL in real applications.¹

2 Problem Formulation

We frame our problem in terms of a constrained Markov Decision Process (CMDP) [16], defined as a tuple $\langle \mathcal{S}, \mathcal{A}, T, R, C \rangle$. Here \mathcal{S} is the set of states, \mathcal{A} is the set of actions, and T specifies the conditional probability $T(s'|s, a)$ that the next state is s' given the current state s and action a . In addition, $R : \mathcal{S} \times \mathcal{A} \rightarrow \mathbb{R}$ is a reward function, and $C : \mathcal{S} \times \mathcal{A} \rightarrow \mathbb{R}$ is a constraint cost function. The reward function encodes the benefit of using action a in state s , while the cost function encodes the corresponding constraint violation penalty.

A policy is a map from states to probability distributions on \mathcal{A} . It specifies that in state s the selected action is drawn from the distribution $\pi(s)$. The state then transits from s to s' according to the state transition distribution $T(s'|s, a)$. In doing so, a reward $R(s, a)$ is received and a constraint cost $C(s, a)$ is incurred, as outlined above.

Let $\gamma \in (0, 1)$ denote a discount factor, and τ denote the trajectory $\tau = (s_0, a_0, s_1, \dots)$ induced by a policy π . Normally, we seek a policy π that maximizes a cumulative discounted reward

$$J_R(\pi) \doteq \mathbb{E}_{\tau \sim \pi} [\sum_{t=0}^{\infty} \gamma^t R(s_t, a_t)], \quad (1)$$

while keeping the cumulative discounted cost below h_C

$$J_C(\pi) \doteq \mathbb{E}_{\tau \sim \pi} [\sum_{t=0}^{\infty} \gamma^t C(s_t, a_t)] \leq h_C. \quad (2)$$

Here we consider an additional objective. We are provided with a baseline policy π_B and at each state s we measure the divergence between $\pi(s)$ and $\pi_B(s)$. For example, this could be the KL-divergence $D(s) \doteq D_{\text{KL}}(\pi(s) \parallel \pi_B(s))$. We then seek a policy that maximizes Eq. (1), satisfies Eq. (2), and ensures the discounted divergence between the learned and baseline policies is below h_D :

$$J_D(\pi) \doteq \mathbb{E}_{\tau \sim \pi} [\sum_{t=0}^{\infty} \gamma^t D(s_t)] \leq h_D. \quad (3)$$

We do not assume that the baseline policy satisfies the cost constraint. Hence we allow h_D to be adjusted during the learning of π to allow for reward improvement and constraint satisfaction.

¹Here is a link to the code: <https://sites.google.com/view/spaceneurips>.

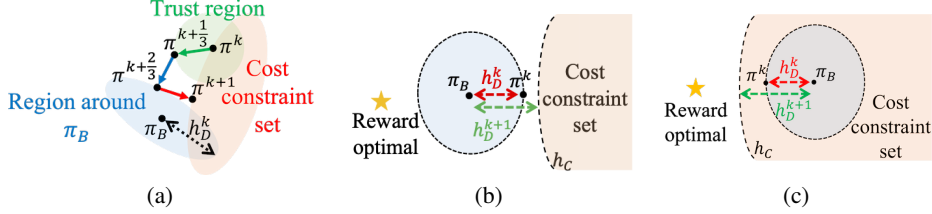


Figure 1: **(a)** Update procedures for SPACE. Step 1 (green) improves the reward in the trust region. Step 2 (blue) projects the policy onto a region around π_B . Step 3 (red) projects the policy onto the cost constraint set. **(b)** Illustrating when π_B is *outside* the cost constraint set. **(c)** Illustrating when π_B is *inside* the cost constraint set. The highest reward is achieved at the yellow star.

Let $\mu_t(\cdot|\pi)$ denote the state distribution at time t under policy π . The discounted state distribution induced by π is defined to be

$$d^\pi(s) \doteq (1 - \gamma) \sum_{t=0}^{\infty} \gamma^t \mu_t(s|\pi).$$

Now bring in the reward advantage function [17] defined by

$$A_R^\pi(s, a) \doteq Q_R^\pi(s, a) - V_R^\pi(s),$$

where $V_R^\pi(s) \doteq \mathbb{E}_{\tau \sim \pi} [\sum_{t=0}^{\infty} \gamma^t R(s_t, a_t) | s_0 = s]$ is the expected reward from state s under policy π , and $Q_R^\pi(s, a) \doteq \mathbb{E}_{\tau \sim \pi} [\sum_{t=0}^{\infty} \gamma^t R(s_t, a_t) | s_0 = s, a_0 = a]$ is the expected reward from state s and initial action a , and thereafter following policy π . These definitions allow us to express the reward performance of one policy π' in terms of another π :

$$J_R(\pi') - J_R(\pi) = \frac{1}{1-\gamma} \mathbb{E}_{s \sim d^{\pi'}, a \sim \pi'} [A_R^\pi(s, a)].$$

Similarly, we can define $A_D^\pi(s, a)$, $Q_D^\pi(s, a)$ and $V_D^\pi(s)$ for the divergence cost, and $A_C^\pi(s, a)$, $Q_C^\pi(s, a)$ and $V_C^\pi(s)$ for the constraint cost.

3 Safe Policy Adaptation with Constrained Exploration

We now describe the proposed iterative three step algorithm illustrated in Fig. 1. In what follows, π^k denotes the learned policy after iteration k , and M denotes a distance measure between policies. For example, M might be the 2-norm of the difference of policy parameters or some average over the states of the KL-divergence of the action policy distributions.

Step 1. We perform one step of trust region policy optimization [10]. This maximizes the reward advantage function $A_R^\pi(s, a)$ over a KL-divergence neighborhood of π^k (*i.e.*, a trust region):

$$\pi^{k+\frac{1}{3}} = \arg \max_{\pi} \mathbb{E}_{s \sim d^{\pi^k}, a \sim \pi} [A_R^{\pi^k}(s, a)] \quad \text{s.t.} \quad \mathbb{E}_{s \sim d^{\pi^k}} [D_{\text{KL}}(\pi(s) || \pi^k(s))] \leq \delta. \quad (4)$$

Step 2. We project $\pi^{k+\frac{1}{3}}$ onto a region around π_B controlled by h_D^k to minimize M :

$$\pi^{k+\frac{2}{3}} = \arg \min_{\pi} M(\pi, \pi^{k+\frac{1}{3}}) \quad \text{s.t.} \quad J_D(\pi^k) + \frac{1}{1-\gamma} \mathbb{E}_{s \sim d^{\pi^k}, a \sim \pi} [A_D^{\pi^k}(s)] \leq h_D^k. \quad (5)$$

Step 3. We project $\pi^{k+\frac{2}{3}}$ onto the set of policies satisfying the cost constraint to minimize M :

$$\pi^{k+1} = \arg \min_{\pi} M(\pi, \pi^{k+\frac{2}{3}}) \quad \text{s.t.} \quad J_C(\pi^k) + \frac{1}{1-\gamma} \mathbb{E}_{s \sim d^{\pi^k}, a \sim \pi} [A_C^{\pi^k}(s, a)] \leq h_C. \quad (6)$$

We select h_D^0 to be small and gradually increase h_D^k at each iteration to expand the region around π_B . Specifically, we make $h_D^{k+1} > h_D^k$ if:

- (a) $J_C(\pi^k) > J_C(\pi^{k-1})$: this increase is to ensure a nonempty intersection between the region around π_B and the cost constraint set (feasibility). See Fig. 1(b).
- (b) $J_R(\pi^k) < J_R(\pi^{k-1})$: this increase gives the next policy more freedom to improve the reward and the cost constraint performance (exploration). See Fig. 1(c).

It remains to determine how to set the new value of h_D^{k+1} . Let \mathcal{U}_1 denote the set of policies satisfying the cost constraint, and \mathcal{U}_2^k denote the set of policies in the region around π_B controlled by h_D^k . Then we have the following Lemma.

Lemma 3.1 (Updating h_D). *If at step $k + 1$*

$$h_D^{k+1} \geq \mathcal{O}((J_C(\pi^k) - h_C)^2) + h_D^k,$$

then $\mathcal{U}_1 \cap \mathcal{U}_2^{k+1} \neq \emptyset$ (feasibility) and $\mathcal{U}_2^{k+1} \cap \partial\mathcal{U}_1 \neq \emptyset$ (exploration).

Proof. See the supplementary material. \square

Lemma 3.1 ensures that the boundaries of the region around π_B determined by h_D and the set of policies satisfying the cost constraint intersect. This allows the learning algorithm to explore policies within the cost constraint set while still learning from the baseline policy.

4 Algorithm Details

We will implement a policy as a neural network with fixed architecture parameterized by $\theta \in \mathbb{R}^n$. We then learn a policy from the achievable set $\{\pi(\cdot|\theta) : \theta \in \mathbb{R}^n\}$ by iteratively learning θ . Let θ^k and $\pi^k \doteq \pi(\cdot|\theta^k)$ denote the parameter value and the corresponding policy at step k . In this setting, it is impractical to solve for the policy updates in Eq. (4), (5) and (6). Hence we approximate the reward function and constraints with first order Taylor expansions, and KL-divergence with a second order Taylor expansion. We will need the following derivatives:

$$\begin{aligned} \mathbf{g}^k &\doteq \nabla_{\theta} \mathbb{E}_{s \sim d^{\pi^k}, a \sim \pi} [A_R^{\pi^k}(s, a)] \text{ (Gradient of the reward advantage function),} \\ \mathbf{a}^k &\doteq \nabla_{\theta} \mathbb{E}_{s \sim d^{\pi^k}, a \sim \pi} [A_D^{\pi^k}(s)] \text{ (Gradient of the divergence advantage function),} \\ \mathbf{c}^k &\doteq \nabla_{\theta} \mathbb{E}_{s \sim d^{\pi^k}, a \sim \pi} [A_C^{\pi^k}(s, a)] \text{ (Gradient of the cost advantage function),} \\ \mathbf{F}^k &\doteq \nabla_{\theta}^2 \mathbb{E}_{s \sim d^{\pi^k}} [D_{\text{KL}}(\pi(s) \parallel \pi^k(s))] \text{ (Hessian of the KL-divergence constraint).} \end{aligned}$$

Each of these derivatives are taken w.r.t. the neural network parameter and evaluated at θ^k . We also define $b^k \doteq J_D(\pi^k) - h_D^k$, and $d^k \doteq J_C(\pi^k) - h_C$.

Step 1. Approximating Eq. (4) yields

$$\theta^{k+\frac{1}{3}} = \arg \max_{\theta} \mathbf{g}^{kT} (\theta - \theta^k) \quad \text{s.t.} \quad \frac{1}{2} (\theta - \theta^k)^T \mathbf{F}^k (\theta - \theta^k) \leq \delta. \quad (7)$$

Step 2 and Step 3. Approximating Eq. (5) and (6), similarly yields

$$\theta^{k+\frac{2}{3}} = \arg \min_{\theta} \frac{1}{2} (\theta - \theta^{k+\frac{1}{3}})^T \mathbf{L} (\theta - \theta^{k+\frac{1}{3}}) \quad \text{s.t.} \quad \mathbf{a}^{kT} (\theta - \theta^k) + b^k \leq 0, \quad (8)$$

$$\theta^{k+1} = \arg \min_{\theta} \frac{1}{2} (\theta - \theta^{k+\frac{2}{3}})^T \mathbf{L} (\theta - \theta^{k+\frac{2}{3}}) \quad \text{s.t.} \quad \mathbf{c}^{kT} (\theta - \theta^k) + d^k \leq 0, \quad (9)$$

where $\mathbf{L} = \mathbf{I}$ for the 2-norm projection and $\mathbf{L} = \mathbf{F}^k$ for the KL-divergence projection.

We solve Problem (7), (8) and (9) using convex programming (see the supplementary material for the derivation). Let $u^k \doteq \sqrt{\frac{2\delta}{\mathbf{g}^{kT} \mathbf{F}^{k-1} \mathbf{g}^k}}$. Then for each policy update, we have

$$\begin{aligned} \theta^{k+1} = \theta^k &+ u^k \mathbf{F}^{k-1} \mathbf{g}^k - \max\left(0, \frac{u^k \mathbf{a}^{kT} \mathbf{F}^{k-1} \mathbf{g}^k + b^k}{\mathbf{a}^{kT} \mathbf{L}^{-1} \mathbf{a}^k}\right) \mathbf{L}^{-1} \mathbf{a}^k \\ &- \max\left(0, \frac{u^k \mathbf{c}^{kT} \mathbf{F}^{k-1} \mathbf{g}^k + d^k}{\mathbf{c}^{kT} \mathbf{L}^{-1} \mathbf{c}^k}\right) \mathbf{L}^{-1} \mathbf{c}^k. \end{aligned} \quad (10)$$

Algorithm 1 shows the corresponding pseudocode.

Convergence Analysis. We consider the following simplified problem to provide a finite-sample guarantee of SPACE:

$$\min_{\theta \in \mathcal{C}_1 \cap \mathcal{C}_2} f(\theta), \quad (11)$$

where $f : \mathbb{R}^n \rightarrow \mathbb{R}$ is a twice continuously differentiable function at every point in an open set $\mathcal{X} \subseteq \mathbb{R}^n$, and $\mathcal{C}_1 \subseteq \mathcal{X}$ and $\mathcal{C}_2 \subseteq \mathcal{X}$ are compact convex sets with $\mathcal{C}_1 \cap \mathcal{C}_2 \neq \emptyset$. The function f is the negative reward function of our CMDP, and the two constraint sets represent the cost constraint set and the region around π_B .

For a vector \mathbf{x} , let $\|\mathbf{x}\|$ denote the Euclidean norm. For a matrix \mathbf{M} let $\|\mathbf{M}\|$ denote the induced matrix 2-norm, and $\sigma_i(\mathbf{M})$ denote the i -th largest singular value of \mathbf{M} .

Assumption 1. We assume:

- (1.1) The gradient ∇f is L -Lipschitz continuous over a open set \mathcal{X} .
- (1.2) For some constant G , $\|\nabla f(\boldsymbol{\theta})\| \leq G$.
- (1.3) For some constant H , $\text{diam}(\mathcal{C}_1) \leq H$ and $\text{diam}(\mathcal{C}_2) \leq H$.

Assumptions (1.1) and (1.2) ensure that the gradient can not change too rapidly and the norm of the gradient can not be too large. Assumption (1.3) implies that for every iteration, the diameter of the region around π_B is bounded above by H .

We will need a concept of an ϵ -first order stationary point [18]. For $\epsilon > 0$, we say that $\boldsymbol{\theta}^* \in \mathcal{C}_1 \cap \mathcal{C}_2$ an ϵ -first order stationary point (ϵ -FOSP) of Problem (11) under KL-divergence projection if

$$\nabla f(\boldsymbol{\theta}^*)^T (\boldsymbol{\theta} - \boldsymbol{\theta}^*) \geq -\epsilon, \quad \forall \boldsymbol{\theta} \in \mathcal{C}_1 \cap \mathcal{C}_2. \quad (12)$$

Similarly, under the 2-norm projection, $\boldsymbol{\theta}^* \in \mathcal{C}_1 \cap \mathcal{C}_2$ an ϵ -FOSP of (11) if

$$\nabla f(\boldsymbol{\theta}^*)^T \mathbf{F}^* (\boldsymbol{\theta} - \boldsymbol{\theta}^*) \geq -\epsilon, \quad \forall \boldsymbol{\theta} \in \mathcal{C}_1 \cap \mathcal{C}_2, \quad (13)$$

where $\mathbf{F}^* \doteq \nabla_{\boldsymbol{\theta}}^2 \mathbb{E}_{s \sim d^{\pi^*}} [D_{\text{KL}}(\pi(s) \parallel \pi^*(s))]$. Notice that SPACE converges to distinct stationary points under the two possible projections (see the supplementary material).

With these assumptions, we have the following Theorem.

Theorem 4.1 (Finite-Sample Guarantee of SPACE). *Under the KL-divergence projection, there exists a sequence $\{\eta^k\}$ such that SPACE converges to an ϵ -FOSP in at most $\mathcal{O}(\epsilon^{-2})$ iterations. Moreover, at step $k + 1$*

$$f(\boldsymbol{\theta}^{k+1}) \leq f(\boldsymbol{\theta}^k) - \frac{L\epsilon^2}{2(G + \frac{H\sigma_1(\mathbf{F}^k)}{\eta^k})^2}. \quad (14)$$

Similarly, under the 2-norm projection, there exists a sequence $\{\eta^k\}$ such that SPACE converges to an ϵ -FOSP in at most $\mathcal{O}(\epsilon^{-2})$ iterations. Moreover, at step $k + 1$

$$f(\boldsymbol{\theta}^{k+1}) \leq f(\boldsymbol{\theta}^k) - \frac{L\epsilon^2}{2(G\sigma_1(\mathbf{F}^{k-1}) + \frac{H}{\eta^k})^2}. \quad (15)$$

Proof. The proof and the sequence $\{\eta^k\}$ are given in the supplementary material. \square

We now make several observations for Theorem 4.1.

(1) The smaller H is, the greater the decrease in the objective. This observation supports the idea of starting with a small value for h_D and increasing it only when needed.

(2) Under the KL-divergence projection, the effect of $\sigma_1(\mathbf{F}^k)$ is negligible. This is because in this case η^k is determined by the KL-divergence between two consecutive updated policies (see the supplementary material). This implies that η^k is proportional to $\sigma_1(\mathbf{F}^k)$. Hence $\sigma_1(\mathbf{F}^k)$ does not play a major role in decreasing the objective value.

(3) Under the 2-norm projection, the smaller $\sigma_1(\mathbf{F}^{k-1})$ (*i.e.*, larger $\sigma_n(\mathbf{F}^k)$) is, the greater the decrease in the objective. This is because a large $\sigma_n(\mathbf{F}^k)$ means a large curvature of f in all directions. This implies that the 2-norm distance between the pre-projection and post-projection points is small, leading to a small deviation from the reward improvement direction after doing projections (see the supplementary material for a visualization).

Algorithm 1 Safe Policy Adaptation with Constrained Exploration (SPACE)

Initialize a policy $\pi^0 = \pi(\cdot | \boldsymbol{\theta}^0)$ and a trajectory buffer \mathcal{B}
for $k = 0, 1, 2, \dots$ **do**
 Run $\pi^k = \pi(\cdot | \boldsymbol{\theta}^k)$ and store trajectories in \mathcal{B}
 Compute $\mathbf{g}, \mathbf{a}, \mathbf{c}, \mathbf{F}, b$ and d using \mathcal{B}
 Obtain $\boldsymbol{\theta}^{k+1}$ using the update in Eq. (10)
 if $J_C(\pi^k) > J_C(\pi^{k-1})$ or $J_R(\pi^k) < J_R(\pi^{k-1})$ **then**
 Update h_D^{k+1} using Lemma 3.1
 Empty \mathcal{B}

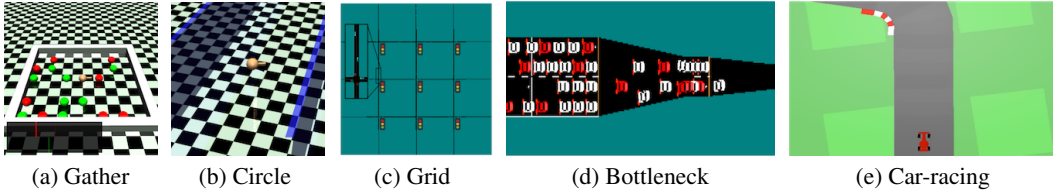


Figure 2: **(a)** Gather task: the agent is rewarded for gathering green apples, but is constrained to collect a limited number of red apples [13]. **(b)** Circle task: the agent is rewarded for moving in a specified wide circle, but is constrained to stay within a safe region smaller than the radius of the circle [13]. **(c)** Grid task: the agent controls the traffic lights in a grid road network and is rewarded for high throughput, but is constrained to let lights stay red for at most 7 consecutive seconds [14]. **(d)** Bottleneck task: the agent controls a set of autonomous vehicles (shown in red) in a traffic merge situation and is rewarded for achieving high throughput, but constrained to ensure that human-driven vehicles (shown in white) have low speed for no more than 10 seconds [14]. **(e)** Car-racing task: the agent controls an autonomous vehicle on a race track and is rewarded for driving through as many tiles as possible, but is constrained to use the brakes at most 5 times to encourage a smooth ride [15].

5 Related Work

Combination of RL and Baseline Policies. Learning constraint-satisfying policies has been explored in the context of safe RL [19]. Prior work has used baseline policies to provide initial information to RL algorithms to reduce or avoid undesirable situations. This is done by either: initializing the policy with the baseline policy [20–23, 6, 24, 25]; or providing a teacher’s advice to the agent [26–29]. However, this work ([30, 31]) often assumes that the baseline policy is constraint-satisfying. In contrast, SPACE can safely leverage the baseline policy without requiring that it satisfies the current constraints.

Evaluation of Demonstration Data. To effectively learn from demonstration data given by the baseline policy, [32, 33, 11] assess the demonstration data by either: predicting their cost in the new application using generative adversarial networks [34]; or directly learning the cost function of the demonstration data. These approaches allow the learning agent to identify which actions given by the baseline policy are constraint-satisfying. However, this requires a large number of training samples from the new application. In addition, the learned cost function is not guaranteed to recover the true one. This may result in driving the agent to undesirable situations. In contrast, SPACE dynamically controls the distance between the learned and baseline policies to ensure reward improvement and constraint satisfaction.

Comparison to PCPO [35]. Perhaps the closest work to ours is the approach of Projection-based Constrained Policy Optimization (PCPO), which proposes using a projection onto the cost constraint set to ensure constraint satisfaction. Since PCPO does not learn from the baseline policy, it is less sample-efficient. In contrast, SPACE leverages the baseline policy to achieve fast learning.

6 Experiments

Tasks. We compare the proposed algorithm with existing approaches on five control tasks: three tasks with safety constraints ((a), (b) and (e) in Fig. 2), and two tasks with fairness constraints ((c) and (d) in Fig. 2). These tasks are briefly described in the caption of Fig. 2. We chose the traffic management tasks since a good control policy can benefit millions of drivers. In addition, we chose the car-racing task since a good algorithm should safely learn from baseline human policies.

Baseline Policies. In the gather, circle, grid, and bottleneck tasks, we pre-train the baseline policies using PCPO [35]. To test whether SPACE can safely leverage the baseline policy, we used three variants of the baseline policies: (1) π_B^{cost} with $J_C(\pi_B^{\text{cost}}) \approx 0$, (2) π_B^{reward} with $J_C(\pi_B^{\text{reward}}) > h_C$, and (3) π_B^{same} with $J_C(\pi_B^{\text{same}}) \approx h_C$ (i.e., the baseline policy has the same cost constraint as the agent). In addition, in the car-racing task we pre-train a baseline policy using an off-policy algorithm (DDPG [36]), which directly learns from human demonstration data. This baseline policy is denoted by π_B^{human} .

Implementation. For all the algorithms, we use neural networks to represent Gaussian policies. We use the KL-divergence projection in the Mujoco and car-racing tasks, and the 2-norm projection in

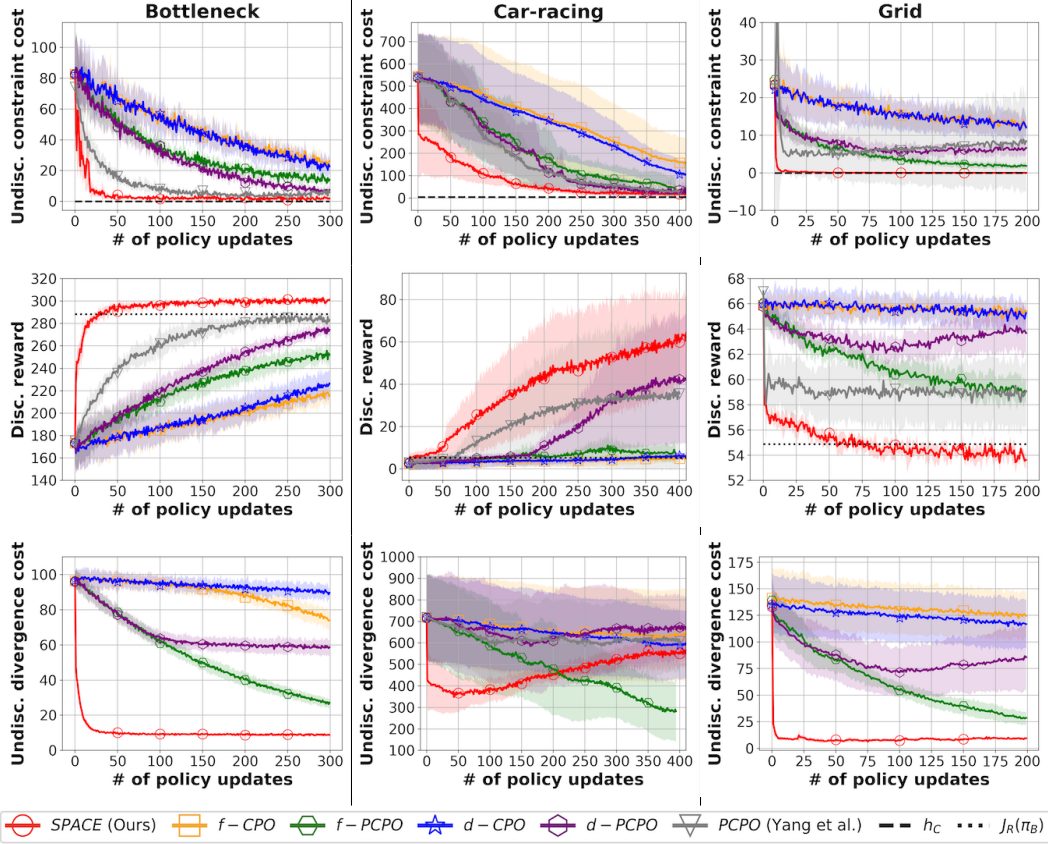


Figure 3: The undiscounted constraint cost, the discounted reward, and the undiscounted divergence cost over policy updates for the tested algorithms and tasks. The solid line is the mean and the shaded area is the standard deviation over 5 runs. The baseline policies in the grid and bottleneck tasks are π_B^{same} , and the baseline policy in the car-racing task is π_B^{human} . Overall, we observe that SPACE is the only algorithm that satisfies the constraints while achieving superior reward performance in all cases. (We test SPACE in all tasks but only show the results in the grid, bottleneck, and car-racing tasks as representative cases since these tasks are more challenging compared to the Mujoco tasks. Please read the supplementary material for more results. Best viewed in color.)

the traffic management task since it achieves better performance. See the supplementary material for the algorithm hyper-parameters and ablation studies.

Baselines. We compare the proposed algorithm with five baselines outlined below.

(1) Fixed-point Constrained Policy Optimization (f-CPO). In f-CPO, the weight λ is fixed followed by a CPO update [13]. A f-CPO policy update solves:

$$\theta^{k+1} = \arg \max_{\theta} (\mathbf{g}^k + \lambda \mathbf{a}^k)^T (\theta - \theta^k) \text{ s.t. } \frac{1}{2} (\theta - \theta^k)^T \mathbf{F}^k (\theta - \theta^k) \leq \delta, \mathbf{c}^k{}^T (\theta - \theta^k) + d^k \leq 0.$$

(2) Fixed-point Projection-based Constrained Policy Optimization (f-PCPO). In f-PCPO, the weight λ is fixed followed by a PCPO update [35]. A f-PCPO policy update solves:

$$\begin{aligned} \theta^{k+\frac{1}{2}} &= \arg \max_{\theta} (\mathbf{g}^k + \lambda \mathbf{a}^k)^T (\theta - \theta^k) \quad \text{s.t. } \frac{1}{2} (\theta - \theta^k)^T \mathbf{F}^k (\theta - \theta^k) \leq \delta, \\ \theta^{k+1} &= \arg \min_{\theta} \frac{1}{2} (\theta - \theta^{k+\frac{1}{2}})^T \mathbf{L} (\theta - \theta^{k+\frac{1}{2}}) \quad \text{s.t. } \mathbf{c}^k{}^T (\theta - \theta^k) + d^k \leq 0. \end{aligned}$$

(3) Dynamic-point Constrained Policy Optimization (d-CPO). A d-CPO update solves f-CPO problem with a stateful $\lambda^{k+1} = (\lambda^k)^\beta$, where $0 < \beta < 1$. This is inspired by [5].

(4) Dynamic-point Projection-based Constrained Policy Optimization (d-PCPO). A d-PCPO update solves f-PCPO problem with a stateful $\lambda^{k+1} = (\lambda^k)^\beta$, where $0 < \beta < 1$. This is inspired by [5].

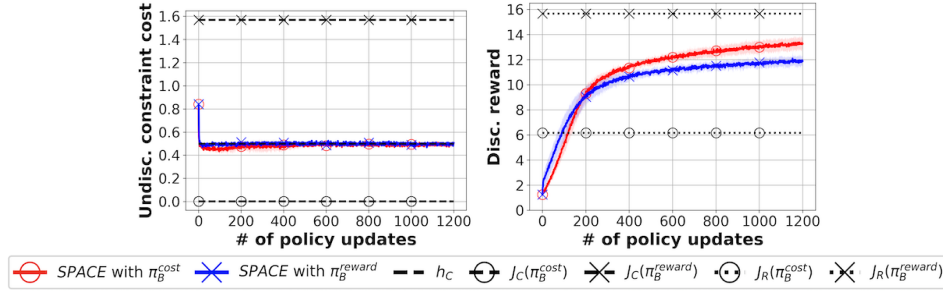


Figure 4: The undiscounted constraint cost and the discounted reward over policy updates for the point gather task. The solid line is the mean and the shaded area is the standard deviation over 5 runs. Learning guided by π_B^{cost} achieves better reward performance. (Best viewed in color.)

(5) Projection-based Constrained Policy Optimization (PCPO) [35]. PCPO is a state-of-the-art algorithm on learning a constraint-satisfying policy. A PCPO update solves f-PCPO problem with $\lambda = 0$. Note that PCPO *ignores* the baseline policy – we treat it as a baseline on the performance.

Overall Performance. The learning curves of the undiscounted constraint cost, the discounted reward, and the undiscounted divergence cost over policy updates are shown for all tested algorithms and tasks in Fig. 3. Please read the caption for more detail about the figure. Overall, we observe that (1) SPACE achieves at least 2 times faster cost constraint satisfaction in all cases, (2) SPACE achieves at least 10% more reward in the bottleneck and car-racing tasks compared to the best baseline, and (3) SPACE is the only algorithm that satisfies the cost constraints in all cases.

For example, in the car-racing task we observe that the value of the divergence cost of SPACE decreases at the initial iteration, but increases in the end. This implies that the learned policy is guided by the baseline policy in the beginning, but use less supervision in the end. In addition, in the grid and the bottleneck tasks we observe that the value of the divergence cost of SPACE converges to a smaller value. This implies that staying close to the baseline policy does not hinder the performance in these tasks. Furthermore, in the grid task we observe that the final reward of SPACE is lower than the baseline. This is because that SPACE converges to a policy in the cost constraint set, whereas the baselines do not find constraint-satisfying policies. These observations show that SPACE can effectively ensure constraint satisfaction while achieving fast learning aided by the baseline policy.

Discussion of f-CPO and f-PCPO. f-CPO and f-PCPO fail to improve the reward and have more cost violations. Most likely this is due to persistent supervision from the baseline policy which need not satisfy the cost constraints nor have high reward. For example, in the car-racing task we observe that the value of the divergence cost decreases throughout the training. This implies that the learned policy overly evolves to the sub-optimal baseline policy and hence degrades the reward performance.

Discussion of d-CPO and d-PCPO. d-CPO and d-PCPO improve the reward slowly and have more cost violations. These approaches do not use projection to quickly learn from the baseline policy. For example, in the car-racing task the value of the divergence cost of d-CPO and d-PCPO are high compared to SPACE throughout the training. This suggests that the agent is not effectively learning from the baseline policy. Hence these approaches require a good selection of the initial value of λ^k .

Comparison of Baseline Policies. The learning curves of the undiscounted constraint cost and the discounted reward over policy updates are shown for the point gather task in Fig. 4. We use two baseline policies: π_B^{cost} and π_B^{reward} , and h_C is set to 0.5. Intuitively, we would expect that learning guided by π_B^{reward} will achieve higher reward. This is because $J_R(\pi_B^{\text{reward}}) > J_R(\pi_B^{\text{cost}})$ as seen in the reward plot. However, we observe that learning guided by π_B^{reward} converges to lower reward. In order to simultaneously satisfy being in a region around π_B^{reward} and in the cost constraint set, SPACE needs extensive back and forth projections onto these sets. This leads to a poor reward improvement direction. In contrast, by starting in the interior of the cost constraint set (*i.e.*, $J_C(\pi_B^{\text{cost}}) \leq h_C$), the agent can safely explore the environment. Although learning guided by π_B^{cost} improves the reward slowly at first, it actually achieves higher reward in the end.

7 Conclusion

We address the problem of learning constraint-satisfying policies given a baseline policy from either a previous application or a teacher. The proposed algorithm uses two projections to effectively learn from the baseline policy without violating the constraints in the new application. SPACE achieves

superior reward and cost performance compared with state-of-the-art approaches. We further analyze the convergence of SPACE and provide an effective approach to controlling the distance between the learned and baseline policies. Future work will consider learning system dynamics to account for the uncertainty of the environment and hence enable safe learning in real applications.

8 Broader Impact

Many autonomous systems such as self-driving cars and autonomous robots are complex. In order to deal with this complexity, researchers are increasingly using reinforcement learning in conjunction with imitation learning for designing control policies. The more we can learn from a previous policy (*e.g.*, human demonstration, previous applications), the fewer resources (*e.g.*, time, energy, engineering effort, cost) we need to learn a new policy. The proposed algorithm could be applied in many fields where learning a policy can take advantage of prior applications while providing assurances for the consideration of fairness, safety, or other costs. For example, in a dialogue system where an agent is intended to converse with a human, the agent should safely learn from human preferences while avoiding producing biased or offensive responses. In addition, in the self-driving car domain where an agent learns a driving policy, the agent should safely learn from human drivers while avoiding a crash. Moreover, in the personalized robotic assistant setting where an agent learns from human demonstration, the agent should carefully imitate humans without damaging itself or causing harm to nearby humans. These examples highlight the potential impact of the proposed algorithm for accelerating safe reinforcement learning by adapting prior knowledge. This can open the door to advances in lifelong learning and adaptation of agents to different contexts.

One deficiency of the proposed algorithm is that the agent still experiments with cost constraint violation when learning control policies. This is because that any learning-based system needs to experiment with various actions to find a constraint-satisfying policy. Even though the agent does not violate the safety constraints during the learning phase, any change or perturbation of the environment that was not envisioned at the time of programming or training may lead to a catastrophic failure during run-time. These systems cannot guarantee that sensor inputs will not induce undesirable consequences, nor can the systems adapt and support safety in situations in which new objectives are created. This creates huge concerns in safety-critical applications such as self-driving vehicles and personalized chatbot system.

This raises several questions: What human-agent communication is needed to bring humans in the loop to increase safety guarantees for the autonomous system? How can trust and safety constraints be incorporated into the planning and control processes? How can one effectively identify unsafe plans of the baseline policy? We believe this paper will encourage future work to develop rigorous design and analysis tools for continual safety assurance in conjunction with using baseline policies from previous applications.

References

- [1] David Silver, Aja Huang, Chris J. Maddison, Arthur Guez, Laurent Sifre, George Van Den Driessche, Julian Schrittwieser, Ioannis Antonoglou, Veda Panneershelvam, Marc Lanctot, et al. Mastering the game of go with deep neural networks and tree search. *Nature*, 529(7587):484, 2016.
- [2] Sergey Levine, Chelsea Finn, Trevor Darrell, and Pieter Abbeel. End-to-end training of deep visuomotor policies. *The Journal of Machine Learning Research*, 17(1):1334–1373, 2016.
- [3] Stéphane Ross, Geoffrey Gordon, and Drew Bagnell. A reduction of imitation learning and structured prediction to no-regret online learning. In *Proceedings of the International Conference on Artificial Intelligence and Statistics*, pages 627–635, 2011.
- [4] Jonathan Ho and Stefano Ermon. Generative adversarial imitation learning. In *Advances in Neural Information Processing Systems*, pages 4565–4573, 2016.
- [5] Aravind Rajeswaran, Vikash Kumar, Abhishek Gupta, Giulia Vezzani, John Schulman, Emanuel Todorov, and Sergey Levine. Learning complex dexterous manipulation with deep reinforcement learning and demonstrations. In *Proceedings of Robotics: Science and Systems*, 2017.

- [6] Yang Gao, Ji Lin, Fisher Yu, Sergey Levine, and Trevor Darrell. Reinforcement learning from imperfect demonstrations. In *Proceedings of the International Conference on Machine Learning*, 2018.
- [7] Todd Hester, Matej Vecerik, Olivier Pietquin, Marc Lanctot, Tom Schaul, Bilal Piot, Dan Horgan, John Quan, Andrew Sendonaris, Ian Osband, et al. Deep q-learning from demonstrations. In *Proceedings of the AAAI Conference on Artificial Intelligence*, 2018.
- [8] Katharina Mülling, Jens Kober, Oliver Kroemer, and Jan Peters. Learning to select and generalize striking movements in robot table tennis. *The International Journal of Robotics Research*, 32(3):263–279, 2013.
- [9] Sonia Chernova and Andrea L. Thomaz. Robot learning from human teachers. *Synthesis Lectures on Artificial Intelligence and Machine Learning*, 8(3):1–121, 2014.
- [10] John Schulman, Sergey Levine, Pieter Abbeel, Michael Jordan, and Philipp Moritz. Trust region policy optimization. In *Proceedings of the International Conference on Machine Learning*, pages 1889–1897, 2015.
- [11] Minae Kwon, Erdem Biyik, Aditi Talati, Karan Bhasin, Dylan P. Losey, and Dorsa Sadigh. When humans aren’t optimal: Robots that collaborate with risk-aware humans. In *Proceedings of ACM/IEEE International Conference on Human-Robot Interaction*, 2020.
- [12] Chen Tessler, Daniel J. Mankowitz, and Shie Mannor. Reward constrained policy optimization. In *Proceedings of the International Conference on Learning Representations*, 2018.
- [13] Joshua Achiam, David Held, Aviv Tamar, and Pieter Abbeel. Constrained policy optimization. In *Proceedings of the International Conference on Machine Learning*, pages 22–31, 2017.
- [14] Eugene Vinitsky, Aboudy Kreidieh, Luc Le Flem, Nishant Kheterpal, Kathy Jang, Cathy Wu, Fangyu Wu, Richard Liaw, Eric Liang, and Alexandre M. Bayen. Benchmarks for reinforcement learning in mixed-autonomy traffic. In *Proceedings of Conference on Robot Learning*, pages 399–409, 2018.
- [15] Greg Brockman, Vicki Cheung, Ludwig Pettersson, Jonas Schneider, John Schulman, Jie Tang, and Wojciech Zaremba. Openai gym. *arXiv preprint arXiv:1606.01540*, 2016.
- [16] Eitan Altman. *Constrained Markov decision processes*, volume 7. CRC Press, 1999.
- [17] Sham Kakade and John Langford. Approximately optimal approximate reinforcement learning. In *Proceedings of the International Conference on Machine Learning*, pages 267–274, 2002.
- [18] Aryan Mokhtari, Asuman Ozdaglar, and Ali Jadbabaie. Escaping saddle points in constrained optimization. In *Advances in Neural Information Processing Systems*, pages 3629–3639, 2018.
- [19] Javier Garcia and Fernando Fernandez. A comprehensive survey on safe reinforcement learning. *Journal of Machine Learning Research*, 16(1):1437–1480, 2015.
- [20] Kurt Driessens and Sašo Džeroski. Integrating guidance into relational reinforcement learning. *Machine Learning*, 57(3):271–304, 2004.
- [21] William D. Smart and Leslie Pack Kaelbling. Practical reinforcement learning in continuous spaces. In *Proceedings of the International Conference on Machine Learning*, pages 903–910. Citeseer, 2000.
- [22] Rogier Koppejan and Shimon Whiteson. Neuroevolutionary reinforcement learning for generalized control of simulated helicopters. *Evolutionary intelligence*, 4(4):219–241, 2011.
- [23] Pieter Abbeel, Adam Coates, and Andrew Y. Ng. Autonomous helicopter aerobatics through apprenticeship learning. *The International Journal of Robotics Research*, 29(13):1608–1639, 2010.
- [24] Hoang M. Le, Cameron Voloshin, and Yisong Yue. Batch policy learning under constraints. In *Proceedings of the International Conference on Machine Learning*, pages 3703–3712, 2019.

- [25] Mel Vecerik, Todd Hester, Jonathan Scholz, Fumin Wang, Olivier Pietquin, Bilal Piot, Nicolas Heess, Thomas Rothörl, Thomas Lampe, and Martin Riedmiller. Leveraging demonstrations for deep reinforcement learning on robotics problems with sparse rewards. *arXiv preprint arXiv:1707.08817*, 2017.
- [26] Javier Garcia and Fernando Fernández. Safe exploration of state and action spaces in reinforcement learning. *Journal of Artificial Intelligence Research*, 45:515–564, 2012.
- [27] Pablo Quintía Vidal, Roberto Iglesias Rodríguez, Miguel Ángel Rodríguez González, and Carlos Vázquez Regueiro. Learning on real robots from experience and simple user feedback. 2013.
- [28] David Abel, John Salvatier, Andreas Stuhlmüller, and Owain Evans. Agent-agnostic human-in-the-loop reinforcement learning. *arXiv preprint arXiv:1701.04079*, 2017.
- [29] Ruohan Zhang, Faraz Torabi, Lin Guan, Dana H. Ballard, and Peter Stone. Leveraging human guidance for deep reinforcement learning tasks. In *Proceedings of the International Joint Conference on Artificial Intelligence*, pages 6339–6346, 2019.
- [30] Wen Sun, Geoffrey J. Gordon, Byron Boots, and Andrew J. Bagnell. Dual policy iteration. In *Advances in Neural Information Processing Systems*, pages 7059–7069, 2018.
- [31] Ashwin Balakrishna, Brijen Thananjeyan, Jonathan Lee, Arsh Zahed, Felix Li, Joseph E. Gonzalez, and Ken Goldberg. On-policy robot imitation learning from a converging supervisor. In *Proceedings of the Conference on Robot Learning*, 2019.
- [32] Yueh-Hua Wu, Nontawat Charoenphakdee, Han Bao, Voot Tangkaratt, and Masashi Sugiyama. Imitation learning from imperfect demonstration. In *Proceedings of the International Conference on Machine Learning*, pages 6818–6827, 2019.
- [33] Daniel S. Brown, Wonjoon Goo, Prabhat Nagarajan, and Scott Niekum. Extrapolating beyond suboptimal demonstrations via inverse reinforcement learning from observations. In *Proceedings of the International Conference on Machine Learning*, pages 783–792, 2019.
- [34] Ian Goodfellow, Jean Pouget-Abadie, Mehdi Mirza, Bing Xu, David Warde-Farley, Sherjil Ozair, Aaron Courville, and Yoshua Bengio. Generative adversarial nets. In *Advances in Neural Information Processing Systems*, pages 2672–2680, 2014.
- [35] Tsung-Yen Yang, Justinian Rosca, Karthik Narasimhan, and Peter J. Ramadge. Projection-based constrained policy optimization. In *Proceedings of the International Conference on Learning Representations*, 2020.
- [36] Timothy P. Lillicrap, Jonathan J. Hunt, Alexander Pritzel, Nicolas Heess, Tom Erez, Yuval Tassa, David Silver, and Daan Wierstra. Continuous control with deep reinforcement learning. In *Proceedings of the International Conference on Learning Representations*, 2016.
- [37] Gong Chen and Marc Teboulle. Convergence analysis of a proximal-like minimization algorithm using bregman functions. *SIAM Journal on Optimization*, 3(3):538–543, 1993.
- [38] John Schulman, Philipp Moritz, Sergey Levine, Michael Jordan, and Pieter Abbeel. High-dimensional continuous control using generalized advantage estimation. In *Proceedings of the International Conference on Learning Representations*, 2016.
- [39] Yan Duan, Xi Chen, Rein Houthoofd, John Schulman, and Pieter Abbeel. Benchmarking deep reinforcement learning for continuous control. In *Proceedings of the International Conference on Machine Learning*, pages 1329–1338, 2016.

Supplementary Material for Accelerating Safe Reinforcement Learning with Constraint-mismatched Policies

Outline. Supplementary material is outlined as follows. Section A details the proof of updating h_D in Lemma 3.1. Section B describes the proof of analytical solution to SPACE in Eq. (10). Section C gives the proof of finite-sample guarantee of SPACE in Theorem 4.1 and discuss the difference between the KL-divergence and 2-norm projections. Section D assembles the additional experiment results to provide a detailed examination of the proposed algorithm compared to the baselines. These include:

- evaluation of the discounted reward versus the cumulative undiscounted constraint cost to demonstrate that SPACE achieves better reward performance with fewer cost constraint violations,
- evaluation of performance of SPACE guided by baseline policies with different $J_C(\pi_B)$ to demonstrate that SPACE safely learns from the baseline policies which need not satisfy the cost constraint,
- ablation studies of using a fixed h_D in SPACE to demonstrate the importance of using the dynamic h_D to improve the reward and cost performance,
- comparison of SPACE and other annealing approaches to demonstrate that SPACE exploits the baseline policy effectively,
- comparison of SPACE under the KL-divergence and the 2-norm projections to demonstrate that they converge to different stationary points,
- evaluation of using different initial values of h_D^0 to demonstrate that the selection of the initial value does not affect the performance of SPACE drastically.

Section D also details the environment parameters, the architectures of policies, computational cost, infrastructure for computation and the instructions for executing the code. Section E provides a procedure for getting a baseline human policy. Finally, we fill the Machine Learning Reproducibility Checklist in Section F.

A Proof of Updating h_D in Lemma 3.1

Proof. Based on Theorem 1 in [13], for any two policies π and π' we have

$$\begin{aligned}
 J_C(\pi') - J_C(\pi) &\geq \frac{1}{1-\gamma} \mathbb{E}_{s \sim d^\pi} \left[A_C^\pi(s, a) - \frac{2\gamma\epsilon_C^{\pi'}}{1-\gamma} \sqrt{\frac{1}{2} D_{\text{KL}}(\pi'(s) \parallel \pi(s))} \right] \\
 \Rightarrow \frac{2\gamma\epsilon_C^{\pi'}}{(1-\gamma)^2} \mathbb{E}_{s \sim d^\pi} \left[\sqrt{\frac{1}{2} D_{\text{KL}}(\pi'(s) \parallel \pi(s))} \right] &\geq -J_C(\pi') + J_C(\pi) + \frac{1}{1-\gamma} \mathbb{E}_{s \sim d^\pi} \left[A_C^\pi(s, a) \right] \\
 \Rightarrow \frac{2\gamma\epsilon_C^{\pi'}}{(1-\gamma)^2} \mathbb{E}_{s \sim d^\pi} \left[\sqrt{\frac{1}{2} D_{\text{KL}}(\pi'(s) \parallel \pi(s))} \right] &\geq -J_C(\pi') + J_C(\pi) \\
 \Rightarrow \frac{\sqrt{2}\gamma\epsilon_C^{\pi'}}{(1-\gamma)^2} \sqrt{\mathbb{E}_{s \sim d^\pi} \left[D_{\text{KL}}(\pi'(s) \parallel \pi(s)) \right]} &\geq -J_C(\pi') + J_C(\pi) \\
 \Rightarrow \mathbb{E}_{s \sim d^\pi} \left[D_{\text{KL}}(\pi'(s) \parallel \pi(s)) \right] &\geq \frac{(1-\gamma)^4 (-J_C(\pi') + J_C(\pi))^2}{2\gamma^2 \epsilon_C^{\pi'^2}}. \tag{16}
 \end{aligned}$$

The fourth inequality follows from Jensen's inequality. We then define $\varphi(\pi(s)) \doteq \sum_i \pi(a(i)|s) \log \pi(a(i)|s)$. By Three-point Lemma [37], for any three policies π, π' , and $\hat{\pi}$ we have

$$\begin{aligned}
 \mathbb{E}_{s \sim d^\pi} \left[D_{\text{KL}}(\pi'(s) \parallel \hat{\pi}(s)) \right] &= \mathbb{E}_{s \sim d^\pi} \left[D_{\text{KL}}(\pi'(s) \parallel \pi(s)) \right] + \mathbb{E}_{s \sim d^\pi} \left[D_{\text{KL}}(\pi(s) \parallel \hat{\pi}(s)) \right] \\
 &\quad - \mathbb{E}_{s \sim d^\pi} \left[(\nabla \varphi(\hat{\pi}(s)) - \nabla \varphi(\pi(s)))^T (\pi'(s) - \pi(s)) \right]. \tag{17}
 \end{aligned}$$

Let π_{boundary} denote a policy satisfying $J_C(\pi_{\text{boundary}}) = h_C$ (i.e., π_{boundary} is in the boundary of the set of the policies which satisfy the cost constraint $J_C(\pi) \leq h_C$). Let $\pi' = \pi_{\text{boundary}}, \hat{\pi} = \pi_B$

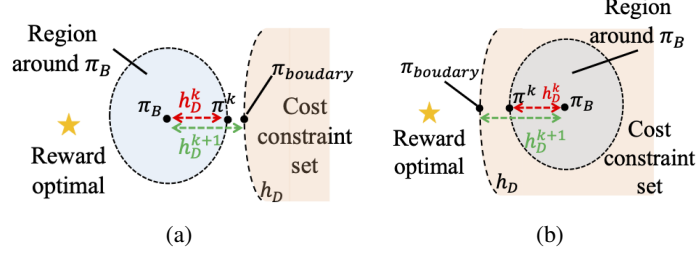


Figure 5: **(a)** Illustrating when π_B is *outside* the cost constraint set. **(b)** Illustrating when π_B is *inside* the cost constraint set. $\pi_{boundary}$ is the policy with $J_C(\pi_{boundary}) = h_C$. We aim to bound h_D^{k+1} (i.e., the KL-divergence between $\pi_{boundary}$ and π_B) by using h_D^k .

and $\pi = \pi^k$ in Eq. (16) and Eq. (17) (this is illustrated in Fig. 5). Then we have

$$\begin{aligned}
& \mathbb{E}_{s \sim d^{\pi^k}} \left[D_{\text{KL}}(\pi_{boundary}(s) || \pi_B(s)) \right] - \mathbb{E}_{s \sim d^{\pi^k}} \left[D_{\text{KL}}(\pi^k(s) || \pi_B(s)) \right] \\
&= \mathbb{E}_{s \sim d^{\pi^k}} \left[D_{\text{KL}}(\pi_{boundary}(s) || \pi^k(s)) \right] \\
&\quad - \mathbb{E}_{s \sim d^{\pi^k}} \left[(\nabla \varphi(\pi_B(s)) - \nabla \varphi(\pi^k(s)))^T (\pi_{boundary}(s) - \pi^k(s)) \right] \\
&\geq \frac{(1-\gamma)^4 (-J_C(\pi_{boundary}) + J_C(\pi^k))^2}{2\gamma^2 \epsilon_C'^2} \\
&\quad - \mathbb{E}_{s \sim d^{\pi^k}} \left[(\nabla \varphi(\pi_B(s)) - \nabla \varphi(\pi^k(s)))^T (\pi_{boundary}(s) - \pi^k(s)) \right] \\
&= \frac{(1-\gamma)^4 (-h_C + J_C(\pi^k))^2}{2\gamma^2 \epsilon_C'^2} \\
&\quad - \mathbb{E}_{s \sim d^{\pi^k}} \left[(\nabla \varphi(\pi_B(s)) - \nabla \varphi(\pi^k(s)))^T (\pi_{boundary}(s) - \pi^k(s)) \right] \\
&= \mathcal{O}\left((-h_C + J_C(\pi^k))^2\right), \tag{18}
\end{aligned}$$

where $J_C(\pi_{boundary}) = h_C$.

For the first case in Fig. 5(a), we would like to have $\mathcal{U}_1 \cap \mathcal{U}_2^{k+1} \neq \emptyset$ (feasibility). For the second case in Fig. 5(b), we would like to have $\mathcal{U}_2^{k+1} \cap \partial \mathcal{U}_1 \neq \emptyset$ (exploration). These implies that the policy in step $k+1$ is $\pi_{boundary}$ which satisfies $\mathcal{U}_1 \cap \mathcal{U}_2^{k+1} \neq \emptyset$ and $\mathcal{U}_2^{k+1} \cap \partial \mathcal{U}_1 \neq \emptyset$.

Now let $h_D^{k+1} \doteq \mathbb{E}_{s \sim d^{\pi^k}} \left[D_{\text{KL}}(\pi_{boundary}(s) || \pi_B(s)) \right]$ and $h_D^k \doteq \mathbb{E}_{s \sim d^{\pi^k}} \left[D_{\text{KL}}(\pi^k(s) || \pi_B(s)) \right]$. Then Eq. 18 implies

$$h_D^{k+1} \geq \mathcal{O}\left((-h_C + J_C(\pi^k))^2\right) + h_D^k.$$

□

B Proof of Analytical Solution to SPACE in Eq. (10)

Proof. For the first problem in Eq. (7), since \mathbf{F}^k is the Fisher Information matrix, it is positive semi-definite. Hence it is a convex program with quadratic inequality constraints. If the primal problem has a feasible point, then Slater's condition is satisfied and strong duality holds. Let θ^* and λ^* denote the solutions to the primal and dual problems, respectively. In addition, the primal objective function is continuously differentiable. Hence the Karush-Kuhn-Tucker (KKT) conditions are necessary and sufficient for the optimality of θ^* and λ^* . We now form the Lagrangian:

$$\mathcal{L}(\theta, \lambda) = -g^k T (\theta - \theta^k) + \lambda \left(\frac{1}{2} (\theta - \theta^k)^T \mathbf{F}^k (\theta - \theta^k) - \delta \right).$$

And we have the following KKT conditions:

$$-\mathbf{g}^k + \lambda^* \mathbf{F}^k \boldsymbol{\theta}^* - \lambda^* \mathbf{F}^k \boldsymbol{\theta}^k = 0 \quad \nabla_{\boldsymbol{\theta}} \mathcal{L}(\boldsymbol{\theta}^*, \lambda^*) = 0 \quad (19)$$

$$\frac{1}{2}(\boldsymbol{\theta}^* - \boldsymbol{\theta}^k)^T \mathbf{F}^k (\boldsymbol{\theta}^* - \boldsymbol{\theta}^k) - \delta = 0 \quad \nabla_{\lambda} \mathcal{L}(\boldsymbol{\theta}^*, \lambda^*) = 0 \quad (20)$$

$$\frac{1}{2}(\boldsymbol{\theta}^* - \boldsymbol{\theta}^k)^T \mathbf{F}^k (\boldsymbol{\theta}^* - \boldsymbol{\theta}^k) - \delta \leq 0 \quad \text{primal constraints} \quad (21)$$

$$\lambda^* \geq 0 \quad \text{dual constraints} \quad (22)$$

$$\lambda^* \left(\frac{1}{2}(\boldsymbol{\theta}^* - \boldsymbol{\theta}^k)^T \mathbf{F}^k (\boldsymbol{\theta}^* - \boldsymbol{\theta}^k) - \delta \right) = 0 \quad \text{complementary slackness} \quad (23)$$

By Eq. (19), we have $\boldsymbol{\theta}^* = \boldsymbol{\theta}^k + \frac{1}{\lambda^*} \mathbf{F}^k{}^{-1} \mathbf{g}^k$. And by plugging Eq. (19) into Eq. (20), we have $\lambda^* = \sqrt{\frac{\mathbf{g}^k{}^T \mathbf{F}^k{}^{-1} \mathbf{g}^k}{2\delta}}$. Hence we have a solution

$$\boldsymbol{\theta}^{k+\frac{1}{3}} = \boldsymbol{\theta}^* = \boldsymbol{\theta}^k + \sqrt{\frac{2\delta}{\mathbf{g}^k{}^T \mathbf{F}^k{}^{-1} \mathbf{g}^k}} \mathbf{F}^k{}^{-1} \mathbf{g}^k, \quad (24)$$

which also satisfies Eq. (21), Eq. (22), and Eq. (23).

For the second problem in Eq. (8), we follow the same procedure for the first problem to form the Lagrangian:

$$\mathcal{L}(\boldsymbol{\theta}, \lambda) = \frac{1}{2}(\boldsymbol{\theta} - \boldsymbol{\theta}^{k+\frac{1}{3}})^T \mathbf{L}(\boldsymbol{\theta} - \boldsymbol{\theta}^{k+\frac{1}{3}}) + \lambda(\mathbf{a}^k{}^T (\boldsymbol{\theta} - \boldsymbol{\theta}^k) + b^k).$$

And we have the following KKT conditions:

$$\mathbf{L}\boldsymbol{\theta}^* - \mathbf{L}\boldsymbol{\theta}^{k+\frac{1}{3}} + \lambda^* \mathbf{a}^k = 0 \quad \nabla_{\boldsymbol{\theta}} \mathcal{L}(\boldsymbol{\theta}^*, \lambda^*) = 0 \quad (25)$$

$$\mathbf{a}^k{}^T (\boldsymbol{\theta}^* - \boldsymbol{\theta}^k) + b^k = 0 \quad \nabla_{\lambda} \mathcal{L}(\boldsymbol{\theta}^*, \lambda^*) = 0 \quad (26)$$

$$\mathbf{a}^k{}^T (\boldsymbol{\theta}^* - \boldsymbol{\theta}^k) + b^k \leq 0 \quad \text{primal constraints} \quad (27)$$

$$\lambda^* \geq 0 \quad \text{dual constraints} \quad (28)$$

$$\lambda^* (\mathbf{a}^k{}^T (\boldsymbol{\theta}^* - \boldsymbol{\theta}^k) + b^k) = 0 \quad \text{complementary slackness} \quad (29)$$

By Eq. (25), we have $\boldsymbol{\theta}^* = \boldsymbol{\theta}^k + \lambda^* \mathbf{L}^{-1} \mathbf{a}^k$. And by plugging Eq. (25) into Eq. (26) and Eq. (28), we have $\lambda^* = \max(0, \frac{\mathbf{a}^k{}^T (\boldsymbol{\theta}^{k+\frac{1}{3}} - \boldsymbol{\theta}^k) + b^k}{\mathbf{a}^k{}^T \mathbf{L}^{-1} \mathbf{a}^k})$. Hence we have a solution

$$\boldsymbol{\theta}^{k+\frac{2}{3}} = \boldsymbol{\theta}^* = \boldsymbol{\theta}^k + \frac{\mathbf{a}^k{}^T (\boldsymbol{\theta}^{k+\frac{1}{3}} - \boldsymbol{\theta}^k) + b^k}{\mathbf{a}^k{}^T \mathbf{L}^{-1} \mathbf{a}^k} \mathbf{L}^{-1} \mathbf{a}^k, \quad (30)$$

which also satisfies Eq. (27) and Eq. (29).

For the third problem in Eq. (9), instead of doing the projection on $\pi^{k+\frac{2}{3}}$ which is the intermediate policy obtained in the second step, we project the policy $\pi^{k+\frac{1}{3}}$ onto the cost constraint. This allows us to compute the projection without too much computational cost. We follow the same procedure for the first and second problems to form the Lagrangian:

$$\mathcal{L}(\boldsymbol{\theta}, \lambda) = \frac{1}{2}(\boldsymbol{\theta} - \boldsymbol{\theta}^{k+\frac{1}{3}})^T \mathbf{L}(\boldsymbol{\theta} - \boldsymbol{\theta}^{k+\frac{1}{3}}) + \lambda(\mathbf{c}^k{}^T (\boldsymbol{\theta} - \boldsymbol{\theta}^k) + d^k).$$

And we have the following KKT conditions:

$$\mathbf{L}\boldsymbol{\theta}^* - \mathbf{L}\boldsymbol{\theta}^{k+\frac{1}{3}} + \lambda^* \mathbf{c}^k = 0 \quad \nabla_{\boldsymbol{\theta}} \mathcal{L}(\boldsymbol{\theta}^*, \lambda^*) = 0 \quad (31)$$

$$\mathbf{c}^k{}^T (\boldsymbol{\theta}^* - \boldsymbol{\theta}^k) + d^k = 0 \quad \nabla_{\lambda} \mathcal{L}(\boldsymbol{\theta}^*, \lambda^*) = 0 \quad (32)$$

$$\mathbf{c}^k{}^T (\boldsymbol{\theta}^* - \boldsymbol{\theta}^k) + d^k \leq 0 \quad \text{primal constraints} \quad (33)$$

$$\lambda^* \geq 0 \quad \text{dual constraints} \quad (34)$$

$$\lambda^* (\mathbf{c}^k{}^T (\boldsymbol{\theta}^* - \boldsymbol{\theta}^k) + d^k) = 0 \quad \text{complementary slackness} \quad (35)$$

By Eq. (31), we have $\boldsymbol{\theta}^* = \boldsymbol{\theta}^k + \lambda^* \mathbf{L}^{-1} \mathbf{c}^k$. And by plugging Eq. (31) into Eq. (32) and Eq. (34), we have $\lambda^* = \max(0, \frac{\mathbf{c}^{kT} (\boldsymbol{\theta}^{k+\frac{1}{3}} - \boldsymbol{\theta}^k) + d^k}{\mathbf{c}^k \mathbf{L}^{-1} \mathbf{c}^k})$. Hence we have a solution

$$\boldsymbol{\theta}^{k+1} = \boldsymbol{\theta}^* = \boldsymbol{\theta}^{k+\frac{1}{3}} - \max(0, \frac{\mathbf{c}^{kT} (\boldsymbol{\theta}^{k+\frac{1}{3}} - \boldsymbol{\theta}^k) + d^k}{\mathbf{c}^k \mathbf{L}^{-1} \mathbf{c}^k}) \mathbf{L}^{-1} \mathbf{c}^k. \quad (36)$$

Hence by combining Eq. (24), Eq. (30) and Eq. (36), we have

$$\begin{aligned} \boldsymbol{\theta}^{k+1} = \boldsymbol{\theta}^k + & \sqrt{\frac{2\delta}{\mathbf{g}^{kT} \mathbf{F}^{k-1} \mathbf{g}^k}} \mathbf{F}^{k-1} \mathbf{g}^k - \max(0, \frac{\sqrt{\frac{2\delta}{\mathbf{g}^{kT} \mathbf{F}^{k-1} \mathbf{g}^k}} \mathbf{a}^{kT} \mathbf{F}^{k-1} \mathbf{g}^k + b^k}{\mathbf{a}^{kT} \mathbf{L}^{-1} \mathbf{a}^k}) \mathbf{L}^{-1} \mathbf{a}^k \\ & - \max(0, \frac{\sqrt{\frac{2\delta}{\mathbf{g}^{kT} \mathbf{F}^{k-1} \mathbf{g}^k}} \mathbf{c}^{kT} \mathbf{F}^{k-1} \mathbf{g}^k + d^k}{\mathbf{c}^k \mathbf{L}^{-1} \mathbf{c}^k}) \mathbf{L}^{-1} \mathbf{c}^k. \end{aligned}$$

□

C Proof of Finite-Sample Guarantee of SPACE in Theorem 4.1

We now describe the reason for choosing two variants of ϵ -FOSP under two possible projections. Let η_R^k denote the step size for the reward, η_D^k denote the step size for the divergence cost, and η_C^k denote the step size for the constraint cost. Without loss of generality, under the KL-divergence projection, at step $k+1$ SPACE does

$$\boldsymbol{\theta}^{k+1} = \boldsymbol{\theta}^k + \eta_R^k \mathbf{F}^{k-1} \mathbf{g}^k - \eta_D^k \mathbf{F}^{k-1} \mathbf{a}^k - \eta_C^k \mathbf{F}^{k-1} \mathbf{c}^k.$$

Similarly, under the 2-norm projection, at step $k+1$ SPACE does

$$\boldsymbol{\theta}^{k+1} = \boldsymbol{\theta}^k + \eta_R^k \mathbf{F}^k \mathbf{g}^k - \eta_D^k \mathbf{a}^k - \eta_C^k \mathbf{c}^k.$$

With this definition, we have the following Lemma.

Lemma C.1 (Stationary Points for SPACE). *Under the KL-divergence projection, SPACE converges to a stationary point $\boldsymbol{\theta}^*$ satisfying*

$$\eta_R^* \mathbf{g}^* = \eta_D^* \mathbf{a}^* + \eta_C^* \mathbf{c}^*.$$

Under the 2-norm projection, SPACE converges to a stationary point $\boldsymbol{\theta}^$ satisfying*

$$\eta_R^* \mathbf{g}^* = \mathbf{F}^* (\eta_D^* \mathbf{a}^* + \eta_C^* \mathbf{c}^*).$$

Proof. Under the KL-divergence projection, by using the definition of a stationary point we have

$$\begin{aligned} \boldsymbol{\theta}^* &= \boldsymbol{\theta}^* + \eta_R^* \mathbf{F}^{*-1} \mathbf{g}^* - \eta_D^* \mathbf{F}^{*-1} \mathbf{a}^* - \eta_C^* \mathbf{F}^{*-1} \mathbf{c}^* \\ \Rightarrow \eta_R^* \mathbf{F}^{*-1} \mathbf{g}^* &= \eta_D^* \mathbf{F}^{*-1} \mathbf{a}^* + \eta_C^* \mathbf{F}^{*-1} \mathbf{c}^* \\ \Rightarrow \eta_R^* \mathbf{g}^* &= \eta_D^* \mathbf{a}^* + \eta_C^* \mathbf{c}^*. \end{aligned}$$

Under the 2-norm projection, by using the definition of a stationary point we have

$$\begin{aligned} \boldsymbol{\theta}^* &= \boldsymbol{\theta}^* + \eta_R^* \mathbf{F}^{*-1} \mathbf{g}^* - \eta_D^* \mathbf{a}^* - \eta_C^* \mathbf{c}^* \\ \Rightarrow \eta_R^* \mathbf{F}^{*-1} \mathbf{g}^* &= \eta_D^* \mathbf{a}^* + \eta_C^* \mathbf{c}^* \\ \Rightarrow \eta_R^* \mathbf{g}^* &= \mathbf{F}^* (\eta_D^* \mathbf{a}^* + \eta_C^* \mathbf{c}^*). \end{aligned}$$

□

Hence Lemma C.1 motivates the need for defining two variants of FOSP.

Before proving Theorem 4.1, we need the following Lemma. Define $\mathcal{P}_C^L(\boldsymbol{\theta}) \doteq \arg \min_{\boldsymbol{\theta}' \in \mathcal{C}} \|\boldsymbol{\theta} - \boldsymbol{\theta}'\|_L^2 = \arg \min_{\boldsymbol{\theta}' \in \mathcal{C}} (\boldsymbol{\theta} - \boldsymbol{\theta}')^T \mathbf{L} (\boldsymbol{\theta} - \boldsymbol{\theta}')$, and $\mathbf{L} = \mathbf{F}^k$ under the KL-divergence projection, and $\mathbf{L} = \mathbf{I}$ under the 2-norm projection.

Lemma C.2 (Contraction of Projection [35]). *For any $\boldsymbol{\theta}$, $\boldsymbol{\theta}^* = \mathcal{P}_C^L(\boldsymbol{\theta})$ if and only if $(\boldsymbol{\theta} - \boldsymbol{\theta}^*)^T \mathbf{L} (\boldsymbol{\theta} - \boldsymbol{\theta}^*) \leq 0, \forall \boldsymbol{\theta}' \in \mathcal{C}$.*

Proof. (\Rightarrow) Let $\boldsymbol{\theta}^* = \mathcal{P}_{\mathcal{C}}^L(\boldsymbol{\theta})$ for a given $\boldsymbol{\theta} \notin \mathcal{C}$, $\boldsymbol{\theta}' \in \mathcal{C}$ be such that $\boldsymbol{\theta}' \neq \boldsymbol{\theta}^*$, and $\alpha \in (0, 1)$. Then we have

$$\begin{aligned} \|\boldsymbol{\theta} - \boldsymbol{\theta}^*\|_{\mathbf{L}}^2 &\leq \|\boldsymbol{\theta} - (\boldsymbol{\theta}^* + \alpha(\boldsymbol{\theta}' - \boldsymbol{\theta}^*))\|_{\mathbf{L}}^2 \\ &= \|\boldsymbol{\theta} - \boldsymbol{\theta}^*\|_{\mathbf{L}}^2 + \alpha^2\|\boldsymbol{\theta}' - \boldsymbol{\theta}^*\|_{\mathbf{L}}^2 - 2\alpha(\boldsymbol{\theta} - \boldsymbol{\theta}^*)^T \mathbf{L}(\boldsymbol{\theta}' - \boldsymbol{\theta}^*) \\ \Rightarrow (\boldsymbol{\theta} - \boldsymbol{\theta}^*)^T \mathbf{L}(\boldsymbol{\theta}' - \boldsymbol{\theta}^*) &\leq \frac{\alpha}{2}\|\boldsymbol{\theta}' - \boldsymbol{\theta}^*\|_{\mathbf{L}}^2. \end{aligned} \quad (37)$$

Since the right hand side of Eq. (37) can be made arbitrarily small for a given α , we have

$$(\boldsymbol{\theta} - \boldsymbol{\theta}^*)^T \mathbf{L}(\boldsymbol{\theta}' - \boldsymbol{\theta}^*) \leq 0, \forall \boldsymbol{\theta}' \in \mathcal{C}.$$

(\Leftarrow) Let $\boldsymbol{\theta}^* \in \mathcal{C}$ be such that $(\boldsymbol{\theta} - \boldsymbol{\theta}^*)^T \mathbf{L}(\boldsymbol{\theta}' - \boldsymbol{\theta}^*) \leq 0, \forall \boldsymbol{\theta}' \in \mathcal{C}$. We show that $\boldsymbol{\theta}^*$ must be the optimal solution. Let $\boldsymbol{\theta}' \in \mathcal{C}$ and $\boldsymbol{\theta}' \neq \boldsymbol{\theta}^*$. Then we have

$$\begin{aligned} \|\boldsymbol{\theta} - \boldsymbol{\theta}'\|_{\mathbf{L}}^2 - \|\boldsymbol{\theta} - \boldsymbol{\theta}^*\|_{\mathbf{L}}^2 &= \|\boldsymbol{\theta} - \boldsymbol{\theta}^* + \boldsymbol{\theta}^* - \boldsymbol{\theta}'\|_{\mathbf{L}}^2 - \|\boldsymbol{\theta} - \boldsymbol{\theta}^*\|_{\mathbf{L}}^2 \\ &= \|\boldsymbol{\theta} - \boldsymbol{\theta}^*\|_{\mathbf{L}}^2 + \|\boldsymbol{\theta}' - \boldsymbol{\theta}^*\|_{\mathbf{L}}^2 - 2(\boldsymbol{\theta} - \boldsymbol{\theta}^*)^T \mathbf{L}(\boldsymbol{\theta}' - \boldsymbol{\theta}^*) - \|\boldsymbol{\theta} - \boldsymbol{\theta}^*\|_{\mathbf{L}}^2 \\ &> 0 \\ \Rightarrow \|\boldsymbol{\theta} - \boldsymbol{\theta}'\|_{\mathbf{L}}^2 &> \|\boldsymbol{\theta} - \boldsymbol{\theta}^*\|_{\mathbf{L}}^2. \end{aligned}$$

Hence, $\boldsymbol{\theta}^*$ is the optimal solution to the optimization problem, and $\boldsymbol{\theta}^* = \mathcal{P}_{\mathcal{C}}^L(\boldsymbol{\theta})$. \square

We now prove Theorem 4.1. Without loss of generality, on each learning episode SPACE updates the reward followed by the alternation of two projections onto the constraint sets (region around π_B and the cost constraint set):

$$\begin{aligned} \boldsymbol{\theta}^{k+\frac{1}{3}} &= \boldsymbol{\theta}^k - \eta^k \mathbf{F}^{-1} \nabla f(\boldsymbol{\theta}^k), \boldsymbol{\theta}^{k+\frac{2}{3}} = \mathcal{P}_{\mathcal{C}_2}(\boldsymbol{\theta}^{k+\frac{1}{3}}), \boldsymbol{\theta}^{k+1} = \mathcal{P}_{\mathcal{C}_1}(\boldsymbol{\theta}^{k+\frac{2}{3}}), \text{ if } \boldsymbol{\theta}^k \in \mathcal{C}_2, \\ \boldsymbol{\theta}^{k+\frac{1}{3}} &= \boldsymbol{\theta}^k - \eta^k \mathbf{F}^{-1} \nabla f(\boldsymbol{\theta}^k), \boldsymbol{\theta}^{k+\frac{2}{3}} = \mathcal{P}_{\mathcal{C}_1}(\boldsymbol{\theta}^{k+\frac{1}{3}}), \boldsymbol{\theta}^{k+1} = \mathcal{P}_{\mathcal{C}_2}(\boldsymbol{\theta}^{k+\frac{2}{3}}), \text{ if } \boldsymbol{\theta}^k \in \mathcal{C}_1, \end{aligned}$$

where η^k is the step size at step k .

Proof. **SPACE under the KL-divergence projection converges to an ϵ -FOSP.** Based on Lemma C.2 under the KL-divergence projection, and setting $\boldsymbol{\theta} = \boldsymbol{\theta}^k - \eta^k \mathbf{F}^{k-1} \nabla f(\boldsymbol{\theta}^k)$, $\boldsymbol{\theta}^* = \boldsymbol{\theta}^{k+\frac{2}{3}}$ and $\boldsymbol{\theta}' = \boldsymbol{\theta}^k$, we have

$$\begin{aligned} (\boldsymbol{\theta}^k - \boldsymbol{\theta}^{k+\frac{2}{3}})^T \mathbf{F}^k (\boldsymbol{\theta}^k - \eta^k \mathbf{F}^{k-1} \nabla f(\boldsymbol{\theta}^k) - \boldsymbol{\theta}^{k+\frac{2}{3}}) &\leq 0 \\ \Rightarrow \nabla f(\boldsymbol{\theta}^k)^T (\boldsymbol{\theta}^{k+\frac{2}{3}} - \boldsymbol{\theta}^k) &\leq -\frac{1}{\eta^k} (\boldsymbol{\theta}^{k+\frac{2}{3}} - \boldsymbol{\theta}^k)^T \mathbf{F}^k (\boldsymbol{\theta}^{k+\frac{2}{3}} - \boldsymbol{\theta}^k). \end{aligned} \quad (38)$$

Based on the L -Lipschitz continuity of gradients and Eq. (38), we have

$$\begin{aligned} f(\boldsymbol{\theta}^{k+\frac{2}{3}}) &\leq f(\boldsymbol{\theta}^k) + \nabla f(\boldsymbol{\theta}^k)^T (\boldsymbol{\theta}^{k+\frac{2}{3}} - \boldsymbol{\theta}^k) + \frac{L}{2} \|\boldsymbol{\theta}^{k+\frac{2}{3}} - \boldsymbol{\theta}^k\|^2 \\ &\leq f(\boldsymbol{\theta}^k) - \frac{1}{\eta^k} (\boldsymbol{\theta}^{k+\frac{2}{3}} - \boldsymbol{\theta}^k)^T \mathbf{F}^k (\boldsymbol{\theta}^{k+\frac{2}{3}} - \boldsymbol{\theta}^k) + \frac{L}{2} \|\boldsymbol{\theta}^{k+\frac{2}{3}} - \boldsymbol{\theta}^k\|^2 \\ &= f(\boldsymbol{\theta}^k) - \frac{L}{2} \|\boldsymbol{\theta}^{k+\frac{2}{3}} - \boldsymbol{\theta}^k\|^2 - \nabla f(\boldsymbol{\theta}^{k+\frac{2}{3}})^T (\boldsymbol{\theta}^{k+1} - \boldsymbol{\theta}^{k+\frac{2}{3}}) - \frac{L}{2} \|\boldsymbol{\theta}^{k+1} - \boldsymbol{\theta}^{k+\frac{2}{3}}\|^2, \end{aligned} \quad (39)$$

where the equality follows by setting δ (i.e., the size of the trust region) such that

$$\eta^k = \frac{(\boldsymbol{\theta}^{k+\frac{2}{3}} - \boldsymbol{\theta}^k)^T \mathbf{F}^k (\boldsymbol{\theta}^{k+\frac{2}{3}} - \boldsymbol{\theta}^k)}{L \|\boldsymbol{\theta}^{k+\frac{2}{3}} - \boldsymbol{\theta}^k\|^2 + \nabla f(\boldsymbol{\theta}^{k+\frac{2}{3}})^T (\boldsymbol{\theta}^{k+1} - \boldsymbol{\theta}^{k+\frac{2}{3}}) + \frac{L}{2} \|\boldsymbol{\theta}^{k+1} - \boldsymbol{\theta}^{k+\frac{2}{3}}\|^2}.$$

Again, based on Lemma C.2, for $\boldsymbol{\theta} \in \mathcal{C}_2$ we have

$$\begin{aligned}
& (\boldsymbol{\theta}^k - \eta^k \mathbf{F}^{k-1} \nabla f(\boldsymbol{\theta}^k) - \boldsymbol{\theta}^{k+\frac{2}{3}}) \mathbf{F}^k (\boldsymbol{\theta} - \boldsymbol{\theta}^{k+\frac{2}{3}}) \leq 0 \\
\Rightarrow & (-\eta^k \mathbf{F}^{k-1} \nabla f(\boldsymbol{\theta}^k))^T \mathbf{F}^k (\boldsymbol{\theta} - \boldsymbol{\theta}^{k+\frac{2}{3}}) \leq -(\boldsymbol{\theta}^k - \boldsymbol{\theta}^{k+\frac{2}{3}})^T \mathbf{F}^k (\boldsymbol{\theta} - \boldsymbol{\theta}^{k+\frac{2}{3}}) \\
\Rightarrow & \nabla f(\boldsymbol{\theta}^k)^T (\boldsymbol{\theta} - \boldsymbol{\theta}^{k+\frac{2}{3}}) \geq \frac{1}{\eta^k} (\boldsymbol{\theta}^k - \boldsymbol{\theta}^{k+\frac{2}{3}})^T \mathbf{F}^k (\boldsymbol{\theta} - \boldsymbol{\theta}^{k+\frac{2}{3}}) \\
\Rightarrow & \nabla f(\boldsymbol{\theta}^k)^T \boldsymbol{\theta} \geq \nabla f(\boldsymbol{\theta}^k)^T \boldsymbol{\theta}^{k+\frac{2}{3}} + \frac{1}{\eta^k} (\boldsymbol{\theta}^k - \boldsymbol{\theta}^{k+\frac{2}{3}})^T \mathbf{F}^k (\boldsymbol{\theta} - \boldsymbol{\theta}^{k+\frac{2}{3}}) \\
\Rightarrow & f(\boldsymbol{\theta}^k)^T (\boldsymbol{\theta} - \boldsymbol{\theta}^k) \geq \nabla f(\boldsymbol{\theta}^k)^T (\boldsymbol{\theta}^{k+\frac{2}{3}} - \boldsymbol{\theta}^k) + \frac{1}{\eta^k} (\boldsymbol{\theta}^k - \boldsymbol{\theta}^{k+\frac{2}{3}})^T \mathbf{F}^k (\boldsymbol{\theta} - \boldsymbol{\theta}^{k+\frac{2}{3}}) \\
& \geq -\|\nabla f(\boldsymbol{\theta}^k)\| \|\boldsymbol{\theta}^{k+\frac{2}{3}} - \boldsymbol{\theta}^k\| - \frac{1}{\eta^k} \|\boldsymbol{\theta}^{k+\frac{2}{3}} - \boldsymbol{\theta}^k\| \|\mathbf{F}^k\| \|\boldsymbol{\theta} - \boldsymbol{\theta}^{k+\frac{2}{3}}\| \\
& \geq -(G + \frac{D\sigma_1(\mathbf{F}^k)}{\eta^k}) \|\boldsymbol{\theta}^{k+\frac{2}{3}} - \boldsymbol{\theta}^k\|, \tag{40}
\end{aligned}$$

where in the last two inequalities we use the property of the norm. Before reaching an ϵ -FOSP, Eq. (40) implies that

$$\begin{aligned}
-\epsilon & \geq \min_{\boldsymbol{\theta} \in \mathcal{C}_2} \nabla f(\boldsymbol{\theta}^k)^T (\boldsymbol{\theta} - \boldsymbol{\theta}^k) \geq -(G + \frac{D\sigma_1(\mathbf{F}^k)}{\eta^k}) \|\boldsymbol{\theta}^{k+\frac{2}{3}} - \boldsymbol{\theta}^k\| \\
\Rightarrow & \|\boldsymbol{\theta}^{k+\frac{2}{3}} - \boldsymbol{\theta}^k\| \geq \frac{\epsilon}{G + \frac{D\sigma_1(\mathbf{F}^k)}{\eta^k}}. \tag{41}
\end{aligned}$$

Based on Eq. (39) and Eq. (41), we have

$$\begin{aligned}
f(\boldsymbol{\theta}^{k+\frac{2}{3}}) & \leq f(\boldsymbol{\theta}^k) - \frac{L}{2} \|\boldsymbol{\theta}^{k+\frac{2}{3}} - \boldsymbol{\theta}^k\|^2 - \nabla f(\boldsymbol{\theta}^{k+\frac{2}{3}})^T (\boldsymbol{\theta}^{k+1} - \boldsymbol{\theta}^{k+\frac{2}{3}}) - \frac{L}{2} \|\boldsymbol{\theta}^{k+1} - \boldsymbol{\theta}^{k+\frac{2}{3}}\|^2 \\
& \leq f(\boldsymbol{\theta}^k) - \frac{L\epsilon^2}{2(G + \frac{D\sigma_1(\mathbf{F}^k)}{\eta^k})^2} - \nabla f(\boldsymbol{\theta}^{k+\frac{2}{3}})^T (\boldsymbol{\theta}^{k+1} - \boldsymbol{\theta}^{k+\frac{2}{3}}) - \frac{L}{2} \|\boldsymbol{\theta}^{k+1} - \boldsymbol{\theta}^{k+\frac{2}{3}}\|^2. \tag{42}
\end{aligned}$$

Based on the L -Lipschitz continuity of gradients, for the projection to the constraint set \mathcal{C}_1 we have

$$f(\boldsymbol{\theta}^{k+1}) \leq f(\boldsymbol{\theta}^{k+\frac{2}{3}}) + \nabla f(\boldsymbol{\theta}^{k+\frac{2}{3}})^T (\boldsymbol{\theta}^{k+1} - \boldsymbol{\theta}^{k+\frac{2}{3}}) + \frac{L}{2} \|\boldsymbol{\theta}^{k+1} - \boldsymbol{\theta}^{k+\frac{2}{3}}\|^2. \tag{43}$$

Combining Eq. (42) with Eq. (43), we have

$$f(\boldsymbol{\theta}^{k+1}) \leq f(\boldsymbol{\theta}^k) - \frac{L\epsilon^2}{2(G + \frac{D\sigma_1(\mathbf{F}^k)}{\eta^k})^2}. \tag{44}$$

Hence it takes $\mathcal{O}(\epsilon^{-2})$ iterations to reach an ϵ -FOSP.

SPACE under the 2-norm projection converges to an ϵ -FOSP. Based on Lemma C.2 under the 2-norm projection, and setting $\boldsymbol{\theta} = \boldsymbol{\theta}^k - \eta^k \mathbf{F}^{k-1} \nabla f(\boldsymbol{\theta}^k)$, $\boldsymbol{\theta}^* = \boldsymbol{\theta}^{k+\frac{2}{3}}$ and $\boldsymbol{\theta}' = \boldsymbol{\theta}^k$, we have

$$\begin{aligned}
& (\boldsymbol{\theta}^k - \boldsymbol{\theta}^{k+\frac{2}{3}})^T (\boldsymbol{\theta}^k - \eta^k \mathbf{F}^{k-1} \nabla f(\boldsymbol{\theta}^k) - \boldsymbol{\theta}^{k+\frac{2}{3}}) \leq 0 \\
\Rightarrow & (\mathbf{F}^{k-1} \nabla f(\boldsymbol{\theta}^k))^T (\boldsymbol{\theta}^{k+\frac{2}{3}} - \boldsymbol{\theta}^k) \leq -\frac{1}{\eta^k} (\boldsymbol{\theta}^{k+\frac{2}{3}} - \boldsymbol{\theta}^k)^T (\boldsymbol{\theta}^{k+\frac{2}{3}} - \boldsymbol{\theta}^k). \tag{45}
\end{aligned}$$

Based on the L -Lipschitz continuity of gradients and Eq. (45), we have

$$\begin{aligned}
f(\boldsymbol{\theta}^{k+\frac{2}{3}}) & \leq f(\boldsymbol{\theta}^k) + \nabla f(\boldsymbol{\theta}^k)^T (\boldsymbol{\theta}^{k+\frac{2}{3}} - \boldsymbol{\theta}^k) + \frac{L}{2} \|\boldsymbol{\theta}^{k+\frac{2}{3}} - \boldsymbol{\theta}^k\|^2 \\
& \leq f(\boldsymbol{\theta}^k) + (\mathbf{F}^{k-1} \nabla f(\boldsymbol{\theta}^k))^T (\boldsymbol{\theta}^{k+\frac{2}{3}} - \boldsymbol{\theta}^k) + Q + \frac{L}{2} \|\boldsymbol{\theta}^{k+\frac{2}{3}} - \boldsymbol{\theta}^k\|^2 \\
& \leq f(\boldsymbol{\theta}^k) - \frac{1}{\eta^k} (\boldsymbol{\theta}^{k+\frac{2}{3}} - \boldsymbol{\theta}^k)^T (\boldsymbol{\theta}^{k+\frac{2}{3}} - \boldsymbol{\theta}^k) + Q + \frac{L}{2} \|\boldsymbol{\theta}^{k+\frac{2}{3}} - \boldsymbol{\theta}^k\|^2 \\
& = f(\boldsymbol{\theta}^k) - \frac{L}{2} \|\boldsymbol{\theta}^{k+\frac{2}{3}} - \boldsymbol{\theta}^k\|^2 - \nabla f(\boldsymbol{\theta}^{k+\frac{2}{3}})^T (\boldsymbol{\theta}^{k+1} - \boldsymbol{\theta}^{k+\frac{2}{3}}) - \frac{L}{2} \|\boldsymbol{\theta}^{k+1} - \boldsymbol{\theta}^{k+\frac{2}{3}}\|^2, \tag{46}
\end{aligned}$$

where $Q := \nabla f(\boldsymbol{\theta}^k)^T(\boldsymbol{\theta}^{k+\frac{2}{3}} - \boldsymbol{\theta}^k) - (\mathbf{F}^{k-1}\nabla f(\boldsymbol{\theta}^k))^T(\boldsymbol{\theta}^{k+\frac{2}{3}} - \boldsymbol{\theta}^k)$, which represents the difference between the gradient and the nature gradient, and the equality follows by setting δ (*i.e.*, the size of the trust region) such that

$$\eta^k = \frac{\|\boldsymbol{\theta}^{k+\frac{2}{3}} - \boldsymbol{\theta}^k\|^2}{L\|\boldsymbol{\theta}^{k+\frac{2}{3}} - \boldsymbol{\theta}^k\|^2 + Q + \nabla f(\boldsymbol{\theta}^{k+\frac{2}{3}})^T(\boldsymbol{\theta}^{k+1} - \boldsymbol{\theta}^{k+\frac{2}{3}}) + \frac{L}{2}\|\boldsymbol{\theta}^{k+1} - \boldsymbol{\theta}^{k+\frac{2}{3}}\|^2}.$$

Again, based on Lemma C.2, for $\boldsymbol{\theta} \in \mathcal{C}_2$ we have

$$\begin{aligned} & (\boldsymbol{\theta}^k - \eta^k \mathbf{F}^{k-1} \nabla f(\boldsymbol{\theta}^k) - \boldsymbol{\theta}^{k+\frac{2}{3}})(\boldsymbol{\theta} - \boldsymbol{\theta}^{k+\frac{2}{3}}) \leq 0 \\ \Rightarrow & (-\eta^k \mathbf{F}^{k-1} \nabla f(\boldsymbol{\theta}^k))^T(\boldsymbol{\theta} - \boldsymbol{\theta}^{k+\frac{2}{3}}) \leq -(\boldsymbol{\theta}^k - \boldsymbol{\theta}^{k+\frac{2}{3}})^T(\boldsymbol{\theta} - \boldsymbol{\theta}^{k+\frac{2}{3}}) \\ \Rightarrow & \nabla f(\boldsymbol{\theta}^k)^T \mathbf{F}^{k-1}(\boldsymbol{\theta} - \boldsymbol{\theta}^{k+\frac{2}{3}}) \geq \frac{1}{\eta^k}(\boldsymbol{\theta}^k - \boldsymbol{\theta}^{k+\frac{2}{3}})^T(\boldsymbol{\theta} - \boldsymbol{\theta}^{k+\frac{2}{3}}) \\ \Rightarrow & \nabla f(\boldsymbol{\theta}^k)^T \mathbf{F}^{k-1} \boldsymbol{\theta} \geq \nabla f(\boldsymbol{\theta}^k)^T \mathbf{F}^{k-1} \boldsymbol{\theta}^{k+\frac{2}{3}} + \frac{1}{\eta^k}(\boldsymbol{\theta}^k - \boldsymbol{\theta}^{k+\frac{2}{3}})^T(\boldsymbol{\theta} - \boldsymbol{\theta}^{k+\frac{2}{3}}) \\ \Rightarrow & \nabla f(\boldsymbol{\theta}^k)^T \mathbf{F}^{k-1}(\boldsymbol{\theta} - \boldsymbol{\theta}^k) \geq \nabla f(\boldsymbol{\theta}^k)^T \mathbf{F}^{k-1}(\boldsymbol{\theta}^{k+\frac{2}{3}} - \boldsymbol{\theta}^k) + \frac{1}{\eta^k}(\boldsymbol{\theta}^k - \boldsymbol{\theta}^{k+\frac{2}{3}})^T(\boldsymbol{\theta} - \boldsymbol{\theta}^{k+\frac{2}{3}}) \\ & \geq -\|\nabla f(\boldsymbol{\theta}^k)\| \|\mathbf{F}^{k-1}\| \|\boldsymbol{\theta}^{k+\frac{2}{3}} - \boldsymbol{\theta}^k\| - \frac{1}{\eta^k} \|\boldsymbol{\theta}^{k+\frac{2}{3}} - \boldsymbol{\theta}^k\| \|\boldsymbol{\theta} - \boldsymbol{\theta}^{k+\frac{2}{3}}\| \\ & \geq -(G\sigma_1(\mathbf{F}^{k-1}) + \frac{D}{\eta^k}) \|\boldsymbol{\theta}^{k+\frac{2}{3}} - \boldsymbol{\theta}^k\|, \end{aligned} \quad (47)$$

where in the last two inequalities we use the property of the norm. Before reaching an ϵ -FOSP, Eq. (47) implies that

$$\begin{aligned} -\epsilon & \geq \min_{\boldsymbol{\theta} \in \mathcal{C}_2} \nabla f(\boldsymbol{\theta}^k)^T \mathbf{F}^{k-1}(\boldsymbol{\theta} - \boldsymbol{\theta}^k) \geq -(G\sigma_1(\mathbf{F}^{k-1}) + \frac{D}{\eta^k}) \|\boldsymbol{\theta}^{k+\frac{2}{3}} - \boldsymbol{\theta}^k\| \\ \Rightarrow & \|\boldsymbol{\theta}^{k+\frac{2}{3}} - \boldsymbol{\theta}^k\| \geq \frac{\epsilon}{(G\sigma_1(\mathbf{F}^{k-1}) + \frac{D}{\eta^k})}. \end{aligned} \quad (48)$$

Based on Eq. (46) and Eq. (48), we have

$$\begin{aligned} f(\boldsymbol{\theta}^{k+\frac{2}{3}}) & \leq f(\boldsymbol{\theta}^k) - \frac{L}{2} \|\boldsymbol{\theta}^{k+\frac{2}{3}} - \boldsymbol{\theta}^k\|^2 - \nabla f(\boldsymbol{\theta}^{k+\frac{2}{3}})^T(\boldsymbol{\theta}^{k+1} - \boldsymbol{\theta}^{k+\frac{2}{3}}) - \frac{L}{2} \|\boldsymbol{\theta}^{k+1} - \boldsymbol{\theta}^{k+\frac{2}{3}}\|^2 \\ & \leq f(\boldsymbol{\theta}^k) - \frac{L\epsilon^2}{2(G\sigma_1(\mathbf{F}^{k-1}) + \frac{D}{\eta^k})^2} - \nabla f(\boldsymbol{\theta}^{k+\frac{2}{3}})^T(\boldsymbol{\theta}^{k+1} - \boldsymbol{\theta}^{k+\frac{2}{3}}) - \frac{L}{2} \|\boldsymbol{\theta}^{k+1} - \boldsymbol{\theta}^{k+\frac{2}{3}}\|^2. \end{aligned} \quad (49)$$

Based on the L -Lipschitz continuity of gradients, for the projection to the constraint set \mathcal{C}_1 we have

$$f(\boldsymbol{\theta}^{k+1}) \leq f(\boldsymbol{\theta}^{k+\frac{2}{3}}) + \nabla f(\boldsymbol{\theta}^{k+\frac{2}{3}})^T(\boldsymbol{\theta}^{k+1} - \boldsymbol{\theta}^{k+\frac{2}{3}}) + \frac{L}{2} \|\boldsymbol{\theta}^{k+1} - \boldsymbol{\theta}^{k+\frac{2}{3}}\|^2. \quad (50)$$

Combining Eq. (49) with Eq. (50), we have

$$f(\boldsymbol{\theta}^{k+1}) \leq f(\boldsymbol{\theta}^k) - \frac{L\epsilon^2}{2(G\sigma_1(\mathbf{F}^{k-1}) + \frac{D}{\eta^k})^2}. \quad (51)$$

Hence it takes $\mathcal{O}(\epsilon^{-2})$ iterations to reach an ϵ -FOSP. \square

Interpretation on Theorem 4.1. We now provide a visualization in Fig. 6 under two possible projections. For each projection, we consider two possible Fisher information matrices. Please read the caption for more detail. In Fig. 6(a) we observe that since the reward improvement and projection steps use the KL-divergence, the resulting two update points with different $\sigma_1(\mathbf{F}^k)$ are similar. In addition, under the 2-norm projection, the larger $\sigma_n(\mathbf{F}^k)$ is, the greater the decrease in the objective. This is because that a large $\sigma_n(\mathbf{F}^k)$ implies a large curvature of f in all directions. Intuitively, this makes the learning algorithm confident about where to update the policy to decrease the objective value greatly. Geometrically, a large $\sigma_n(\mathbf{F}^k)$ makes the 2-norm distance between the pre-projection and post-projection points small, leading to a small deviation from the reward improvement direction. This is illustrated in Fig. 6(b). We observe that since \mathbf{F}^k determines the curvature of f and the 2-norm projection is used, the updated point with a larger $\sigma_n(\mathbf{F}^k)$ (red dot) achieves more improvement of

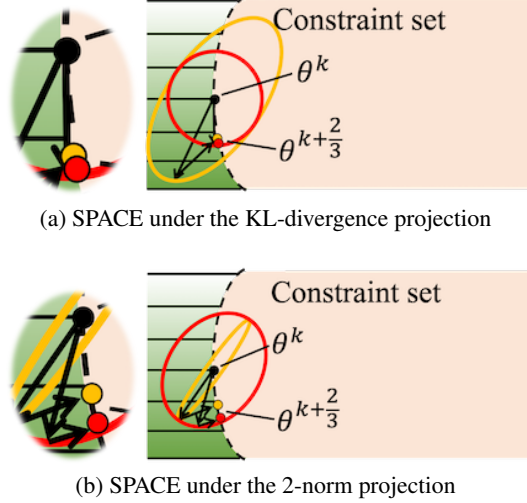


Figure 6: Update procedures for SPACE under the KL and 2-norm projections with two possible Fisher information matrices. A lower objective value is achieved at the darker green area. Red and orange ellipses are \mathbf{F}^k s with two different spectra of singular values. Red and orange dots are resulting updated points under these two spectra of \mathbf{F}^k s. **(a)** A red ellipse has a smaller $\sigma_1(\mathbf{F}^k)$ and an orange ellipse has a larger $\sigma_1(\mathbf{F}^k)$. Both ellipses have the same $\sigma_n(\mathbf{F}^k)$. The two resulting $\theta^{k+\frac{2}{3}}$ are similar. **(b)** A red ellipse has a larger $\sigma_n(\mathbf{F}^k)$ and an orange ellipse has a smaller $\sigma_n(\mathbf{F}^k)$. Both ellipses have the same $\sigma_1(\mathbf{F}^k)$. $\theta^{k+\frac{2}{3}}$ with a larger $\sigma_n(\mathbf{F}^k)$ (red dot) has greater decrease of the objective value.

the objective value. These observations imply that the spectrum of the Fisher information matrix does not play a major role in SPACE under the KL-divergence projection, whereas it affects the decrease of objective value in SPACE under the 2-norm projection. Hence we choose either KL-divergence or 2-norm projections depending on the tasks to achieve better performance.

D Additional Experiment Results

D.1 Implementation Details

Mujoco Task [13]. In the point circle and ant circle tasks, the reward and cost functions are

$$R(s) = \frac{\mathbf{v}^T[-x_2; x_1]}{1 + \|[x_1; x_2]\| - d},$$

and

$$C(s) = \mathbb{1}[|x_1| > x_{\text{lim}}],$$

where x_1 and x_2 are the coordinates in the plane, \mathbf{v} is the velocity of the agent, and d , x_{lim} are environmental parameters that specify the safe area. The agent is rewarded for moving fast in a wide circle with radius of d , but is constrained to stay within a safe region smaller than the radius of the circle in x_1 -coordinate $x_{\text{lim}} \leq d$. For the point agent, we use $d = 5$ and $x_{\text{lim}} = 2.5$; for the ant agent, we use $d = 5$ and $x_{\text{lim}} = 1$. The environment is illustrated in Fig. 7.

In the point gather task, the agent receives a reward of +10 for gathering green apples, and a cost of 1 for gathering red apples. Two green apples and eight red apples are placed in the environment at the beginning. In the ant gather task, the agent receives a reward of +10 for gathering green apples, and a cost of 1 for gathering red apples. The agent also gets a reward of -10 for falling down to encourage smooth moving. Eight green apples and eight red apples are placed in the environment at the beginning.

For the point and ant agents, the state space consists of the positions, orientations, velocities, and the external forces applied to the torso and joint angles. The action space is the force applied to joints.

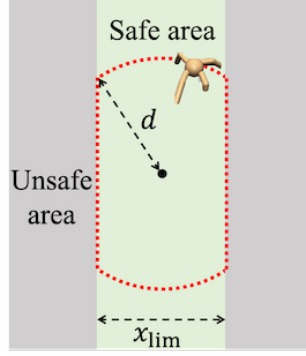


Figure 7: The environment of the circle task (adapted from [13]). The agent receives the maximum reward while staying in the safe area by following the red dashed line path.

Traffic Management Task [14]. In the grid task, the state space, action space, reward function, and cost function are illustrated as follows.

(1) States: Speed, distance to the intersection, and edge number of each vehicle. The edges of the grid are uniquely numbered so the travel direction can be inferred. For the traffic lights, we return 0 and 1 corresponding to green or red for each light, a number between $[0, t_{\text{switch}}]$ indicating how long until a switch can occur, and 0 and 1 indicating if the light is currently yellow. Finally, we return the average density and velocity of each edge.

(2) Actions: A list of numbers $a = [-1, 1]^n$ where n is the number of traffic lights. If $a_i > 0$ for traffic light i it switches, otherwise no action is taken.

(3) Reward: The objective of the agent is to achieve high speeds. The reward function is

$$R(s) = \frac{\max(v_{\text{target}} - \|\mathbf{v}_{\text{target}} - \mathbf{v}\|, 0)}{v_{\text{target}}},$$

where v_{target} is an arbitrary large velocity used to encourage high speeds and $\mathbf{v} \in \mathbb{R}^k$ is the velocities of k vehicles in the network.

(4) Cost: The objective of the agent is to let lights stay red for at most 7 consecutive seconds. The cost function is

$$C(s) = \sum_{i=1}^n \mathbb{1}[t_{i,\text{red}} > 7],$$

where $t_{i,\text{red}}$ is the consecutive time that the light i is in red.

In the bottleneck task, the state space, action space, reward function, and cost function are illustrated as follows.

(1) States: The states include: the mean positions and velocities of human drivers for each lane for each edge segment, the mean positions and velocities of the autonomous vehicles on each segment, and the outflow of the system in vehicles per/hour over the last 5 seconds.

(2) Actions: For a given edge-segment and a given lane, the action shifts the maximum speed of all the autonomous vehicles in the segment from their current value. By shifting the max-speed to higher or lower values, the system indirectly controls the velocity of the autonomous vehicles.

(3) Reward: The objective of the agent is to maximize the outflow of the whole traffic. The reward function is

$$R(s_t) = \sum_{i=t-\frac{5}{\Delta t}}^{i=t} \frac{n_{\text{exit}}(i)}{\Delta t \cdot n_{\text{lane}} \cdot 500},$$

where $n_{\text{exit}}(i)$ is the number of vehicles that exit the system at time-step i , and n_{lane} is the number of lanes.

(4) Cost: The objective of the agent is to let the velocities of human drivers have low speed for no more than 10 seconds. The cost function is

$$C(s) = \sum_{i=1}^{n_{\text{human}}} \mathbb{1}[t_{i,\text{low}} > 10],$$

where n_{human} is the number of human drivers, and $t_{i,\text{low}}$ is the consecutive time that the velocity of human driver i is less than 5 m/s. For more information, please refer to [14].

Car-racing Task. In the car-racing task, the state space, action space, reward function, and the cost function are illustrated as follows.

(1) States: It is a high-dimensional space where the state is a $96 \times 96 \times 3$ tensor of raw pixels. Each pixel is in the range of $[0, 255]$.

(2) Actions: The agent has 12 actions in total: $a \in \mathcal{A} = \{(a^{\text{steer}}, a^{\text{gas}}, a^{\text{brake}}) | a^{\text{steer}} \in \{-1, 0, 1\}, a^{\text{gas}} \in \{0, 1\}, a^{\text{brake}} \in \{0, 0.2\}\}$, where a^{steer} is the steering angle, a^{gas} is the amount of gas applied, and a^{brake} is the amount of brake applied.

(3) Reward: In each episode, we randomly generate the track. The episode is terminated if the agent reaches the maximal step or traverse over 95% of the track. The track is discretized into 281 tiles. The agent receives a reward of $\frac{1000}{281}$ for each tile visited. To encourage driving efficiency, the agent receives a penalty of -1 per-time step.

(4) Cost: The cost is to constrain the accumulated number of brakes to encourage a smooth ride.

Architectures and Parameters. For the gather and circle tasks we test two distinct agents: a point-mass ($S \subseteq \mathbb{R}^9, A \subseteq \mathbb{R}^2$), and an ant robot ($S \subseteq \mathbb{R}^{32}, A \subseteq \mathbb{R}^8$). The agent in the grid task is $S \subseteq \mathbb{R}^{156}, A \subseteq \mathbb{R}^4$, and the agent in the bottleneck task is $S \subseteq \mathbb{R}^{141}, A \subseteq \mathbb{R}^{20}$. Finally, the agent in the car-racing task is $S \subseteq \mathbb{R}^{96 \times 96 \times 3}, A \subseteq \mathbb{R}^3$.

For the simulations in the gather and circle tasks, we use a neural network with two hidden layers of size (64, 32) to represent Gaussian policies. And we use the KL-divergence projection. For the simulations in the grid and bottleneck tasks, we use a neural network with two hidden layers of size (16, 16) and (50, 25) to represent Gaussian policies, respectively. And we use the 2-norm projection. For the simulation in the car-racing task, we use a convolutional neural network with two convolutional operators of size 24 and 12 followed by a dense layer of size (32, 16) to represent a Gaussian policy. And we use the KL-divergence projection. The choice of the projections depends on the task itself, we report the best performance among two projections. We use tanh as an activation function for all the neural network policies. In the experiments, since the step size is small, we reuse the Fisher information matrix of the reward improvement step in the KL-divergence projection step to reduce the computational cost.

We use GAE- λ approach [38] to estimate $A_R^\pi(s, a)$, $A_C^\pi(s, a)$, and $A_D^\pi(s)$. For the simulations in the gather, circle, and car-racing tasks, we use neural network baselines with the same architecture and activation functions as the policy networks. For the simulations in the grid and bottleneck tasks, we use linear baselines. The hyperparameters of all algorithms and all tasks are in Table 1.

We conduct the experiments on three separate machines: machine A has an Intel Core i7-4770HQ CPU, machine B has an Intel Core i7-6850K CPU, and machine C has an Intel Xeon X5675 CPU. We report real-time (*i.e.*, wall-clock time) in seconds for one policy update for all tested algorithms and tasks in Table 2. We observe that SPACE has the same computational time as the other baselines.

For the most intensive task, *i.e.*, the car-racing task, the memory usage is 6.28GB. The experiments are implemented in rllab [39], a tool for developing RL algorithms. We provide the link to the code: <https://sites.google.com/view/spaceneurips>.

Implementation of Updating h_D^k . Lemma 3.1 shows that h_D^{k+1} should be increased at least by $\mathcal{O}((J_C(\pi^k) - h_C)^2) + h_D^k$ if $J_C(\pi^k) > J_C(\pi^{k-1})$ or $J_R(\pi^k) < J_R(\pi^{k-1})$ at step k . We now provide the practical implementation. For each policy update we check the above conditions. If one of the conditions satisfies, we increase h_D^{k+1} by setting the constant to 10, *i.e.*, $10 \cdot (J_C(\pi^k) - h_C)^2 + h_D^k$. In practice, we find that the performance of SPACE is not affected by the selection of the constant.

| Parameter | PC | PG | AC | AG | Gr | BN | CR |
|--|-----------|-----------|-----------|-----------|-----------|-----------|--------------------|
| Reward dis. factor γ | 0.995 | 0.995 | 0.995 | 0.995 | 0.999 | 0.999 | 0.990 |
| Constraint cost dis. factor γ_C | 1.0 | 1.0 | 1.0 | 1.0 | 1.0 | 1.0 | 1.0 |
| Divergence cost dis. factor γ_D | 1.0 | 1.0 | 1.0 | 1.0 | 1.0 | 1.0 | 1.0 |
| step size δ | 10^{-4} | 10^{-4} | 10^{-4} | 10^{-4} | 10^{-4} | 10^{-4} | 5×10^{-4} |
| λ^{GAE} | 0.95 | 0.95 | 0.95 | 0.95 | 0.97 | 0.97 | 0.95 |
| λ_C^{GAE} | 1.0 | 1.0 | 0.5 | 0.5 | 0.5 | 1.0 | 1.0 |
| λ_D^{GAE} | 0.95 | 0.95 | 0.95 | 0.95 | 0.90 | 0.90 | 0.95 |
| Batch size | 50,000 | 50,000 | 100,000 | 100,000 | 10,000 | 25,000 | 10,000 |
| Rollout length | 50 | 15 | 500 | 500 | 400 | 500 | 1000 |
| Constraint cost threshold h_C | 5 | 0.5 | 5 | 0.2 | 0 | 0 | 5 |
| Divergence cost threshold h_D^0 | 5 | 3 | 5 | 3 | 10 | 10 | 5 |
| Number of policy updates | 1,000 | 1,200 | 2,500 | 1,500 | 200 | 300 | 600 |

Table 1: Parameters used in all tasks. (PC: point circle, PG: point gather, AC: ant circle, AG: ant gather, Gr: grid, BN: bottleneck, and CR: car-racing tasks)

| | PCPO | | SPACE (Ours) | | f-PCPO | | f-CPO | | d-PCPO | | d-CPO | |
|----|------|-------|--------------|-------|--------|--------|-------|-------|--------|--------|-------|-------|
| | M/C | Time | M/C | Time | M/C | Time | M/C | Time | M/C | Time | M/C | Time |
| PG | B | 22.14 | B | 25.2 | B | 31.9 | B | 25.5 | B | 32.8 | B | 32.6 |
| PC | B | 35.1 | B | 51.2 | B | 48.4 | B | 49.4 | B | 55.5 | B | 55.9 |
| AG | B | 386.9 | B | 110.5 | C | 268.6 | C | 235.1 | B | 138.2 | B | 187.5 |
| AC | B | 148.9 | B | 94.0 | C | 222.6 | C | 214.6 | B | 177.4 | B | 151.2 |
| Gr | A | 105.3 | A | 91.4 | A | 88.2 | A | 58.7 | A | 116.8 | A | 115.3 |
| BN | A | 257.7 | A | 181.1 | A | 162.9 | A | 161.6 | A | 259.3 | A | 275.6 |
| CR | C | 993.5 | C | 971.6 | C | 1078.3 | C | 940.1 | C | 1000.4 | C | 981.0 |

Table 2: Real-time in seconds for one policy update for all tested algorithms and tasks. (PC: point circle, PG: point gather, AC: ant circle, AG: ant gather, Gr: grid, BN: bottleneck, and CR: car-racing tasks)

Note that we could still compute the exact value of h_D^{k+1} as shown in the proof of Lemma 3.1. However, this incurs the computational cost.

Instructions for Reproducibility. We now provide the instructions for reproducing the results. First install the libraries for python3 such as numpy, scipy. To run the Mujoco experiments, get the licence from <https://www.roboti.us/license.html>. To run the traffic management experiments, install FLOW simulator from <https://flow.readthedocs.io/en/latest/>. To run the car-racing experiments, install OpenAI Gym from <https://github.com/openai/gym>. Our implementation is based on the environment from [13], please download the code from <https://github.com/jachiam/cpo>. The code is based on rllab [39], install the relevant packages such as theano (<http://deeplearning.net/software/theano/>). Then, download SPACE code from <https://sites.google.com/view/spaceneurips> and place the codes on the designated folder instructed by Readme.txt on the main folder. Finally, go to the example folder and execute the code using python command.

D.2 Experiment Results

The Discounted Reward vs. the Cumulative Undiscounted Constraint Cost (see Fig. 8). To show that SPACE achieves higher reward under the same cost constraint violations (*i.e.*, learning a constraint-satisfying policy without violating the cost constraint a lot), we examine the discounted reward versus the *cumulative* undiscounted constraint cost. The learning curves of the discounted reward versus the cumulative undiscounted constraint cost are shown for all tested algorithms and tasks in Fig. 8. We observe that in these tasks under the same value of the reward, SPACE outperforms the baselines significantly with fewer cost constraint violations. For example, in the car-racing task SPACE achieves 3 times fewer cost constraint violations at the reward value of 40 compared to the best baseline – PCPO. This implies that SPACE effectively leverages the baseline policy while ensuring the constraint satisfaction. In contrast, without the supervision of the baseline policy, PCPO requires much more constraint violations to achieve the same reward performance as SPACE. In addition, although the fixed-point and the dynamic-point approaches use the supervision of the baseline policy, the lack of the projection step makes them less efficient in learning a constraint-satisfying policy.

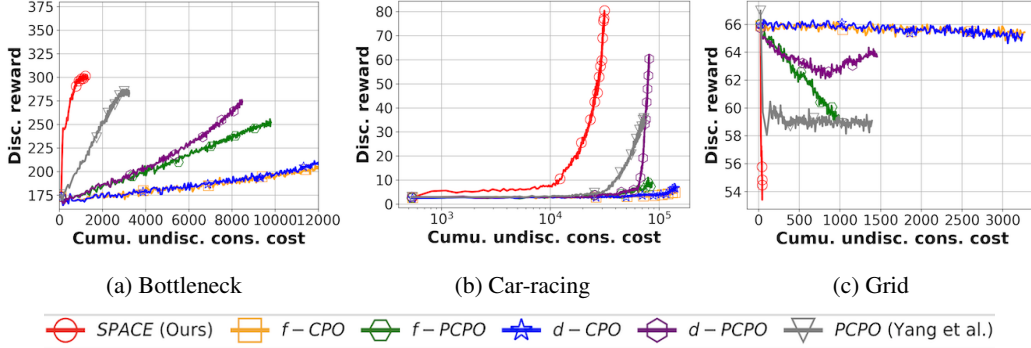


Figure 8: The discounted reward vs. the cumulative undiscounted constraint cost over policy updates for the tested algorithms and tasks. The solid line is the mean over 5 runs. SPACE achieves the same reward performance with fewer cost constraint violations in all cases. (Best viewed in color.)

Comparison of Baseline Policies (see Fig. 9). To examine whether SPACE can safely learn from the baseline policy which need not satisfy the cost constraint, we consider two baseline policies: π_B^{cost} and π_B^{reward} . The learning curves of the undiscounted constraint cost, the discounted reward, and the undiscounted divergence cost with two possible baselines over policy updates are shown for all tested algorithms and tasks in Fig. 9. We observe that in the point gather and point circle tasks, the initial values of the cost are larger than h_C (i.e., $J_C(\pi^0) > h_C$). Using π_B^{cost} allows the learning algorithm to quickly satisfy the cost without doing the extensive projection onto the cost constraint set. For example, in the point circle task we observe that learning guided by π_B^{cost} quickly satisfies the cost constraint. In addition, we observe that in the ant gather and ant circle tasks, the initial values of the cost are smaller than h_C (i.e., $J_C(\pi^0) < h_C$). Intuitively, we would expect that using π_B^{reward} allows the agent to quickly improve the reward since the agent already satisfies the cost constraint in the beginning. In the ant gather task we observe that SPACE guided by π_B^{reward} does improve the reward more quickly at around 200 iteration. However, we observe that the agent guided by the both baseline policies achieve the same final reward performance in the ant gather and ant circle tasks. The reason is that using dynamic h_D allows the agent to stay away from the baseline policy. This makes the baseline policy less influential in the end. As a result, the reward improvement mostly comes from the reward improvement step of SPACE if the agent starts in the interior of the cost constraint set (i.e., $J_C(\pi^0) \leq h_C$).

Fixed h_D (see Fig. 10). To understand the effect of using dynamic h_D^k when learning from a sub-optimal baseline policy, we compare the performance of SPACE with and without adjusting h_D . The learning curves of the undiscounted constraint cost, the discounted reward, and the undiscounted divergence cost over policy updates are shown for all tested algorithms and tasks in Fig. 10. We observe that SPACE with fixed h_D converges to less reward. For example, in the ant circle task SPACE with the dynamic h_D achieves 2.3 times more reward. The value of the divergence cost in the ant circle task shows that staying away from the baseline policy achieves more reward. This implies that the baseline policy in the ant circle task is highly sub-optimal to the agent. In addition, we observe that in some tasks the dynamic h_D does not have much effect on the reward performance. For example, in the point gather task SPACE achieves the same reward performance. The values of the divergence cost in the point gather task decrease throughout the training. These observations imply that the update scheme of h_D is critical for some tasks.

Comparison of SPACE vs. d-CPO, d-PCPO and the Pre-training Approach (see Fig. 11). To show that SPACE is effective in using the supervision of the baseline policy, we compare the performance of SPACE to the dynamic-point and the pre-training approaches. In the pre-training approach, the agent first performs the trust region update with the objective function being the divergence cost. Once the agent has the same reward performance as the baseline policy (i.e., $J_R(\pi^k) \approx J_R(\pi_B)$ for some k), the agent performs the trust region update with the objective function being the reward function. The learning curves of the undiscounted constraint cost, the discounted reward, and the undiscounted divergence cost over policy updates are shown for all tested algorithms and tasks in Fig. 11. We observe that SPACE achieves better reward performance compared to the pre-training approach in all tasks. For example, in the point circle, ant gather and ant circle tasks the

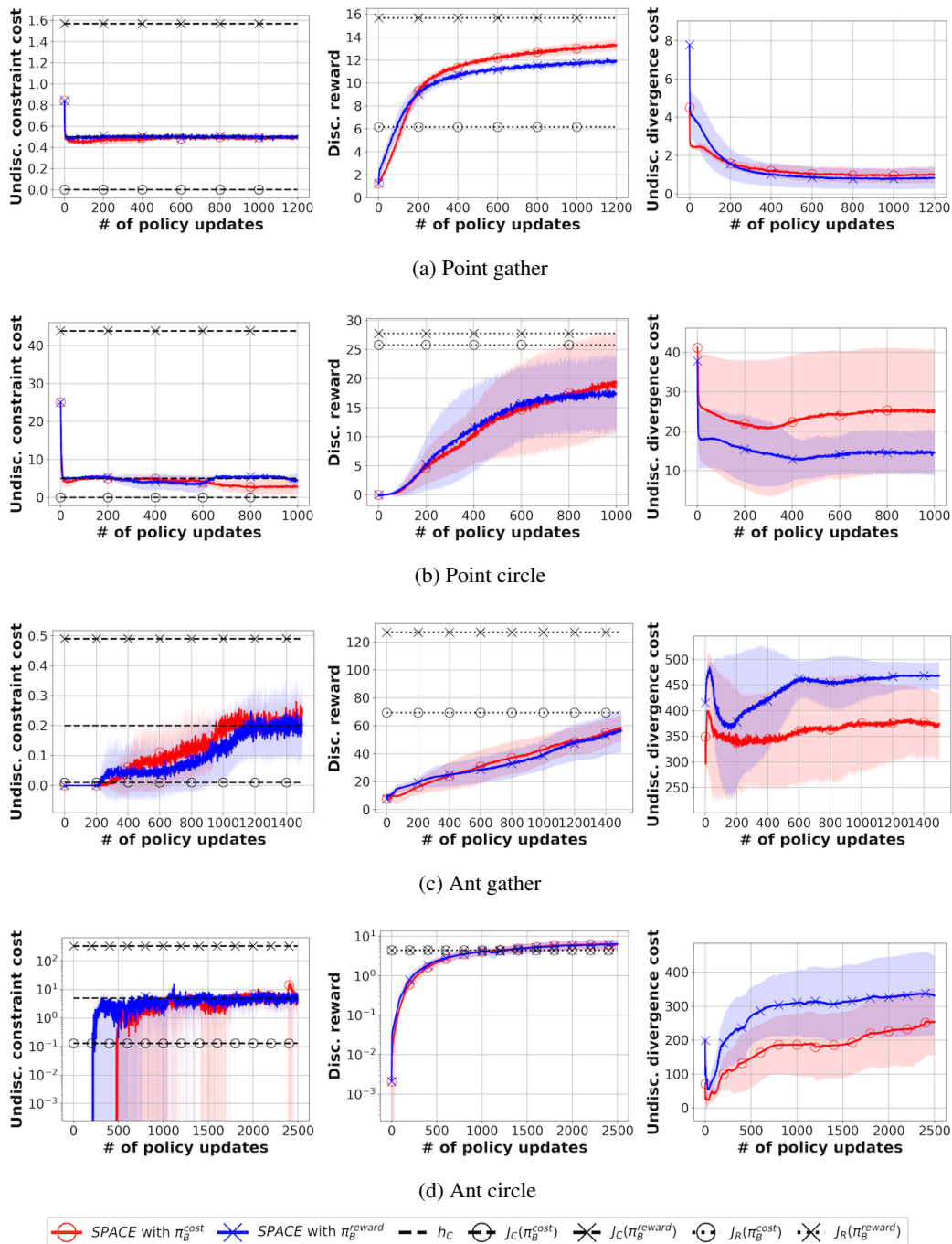


Figure 9: The undiscounted constraint cost, the discounted reward, and the undiscounted divergence cost over policy updates for the tested algorithms and tasks. The solid line is the mean and the shaded area is the standard deviation over 5 runs. SPACE ensures cost constraint satisfaction guided by the baseline policy which need not satisfy the cost constraint. (Best viewed in color.)

pre-training approach seldom improves the reward but all satisfies the cost constraint. This implies that the baseline policies in these tasks are highly sub-optimal in terms of reward performance. In contrast, SPACE prevents the agent from converging to a poor policy.

In addition, we observe that in the point gather task the pre-training approach achieves the same reward performance as the baseline policy, whereas SPACE has a better reward performance compared to the baseline policy. The pre-training approach does not keep improving the reward after learning from the baseline policy. This is because that after pre-training with the baseline policy, the entropy of the learned policy is small. This prevents the agent from trying new actions which may lead to

better reward performance. This implies that pre-training approach may hinder the exploration of the learning agent on the new environment. Furthermore, in the car-racing task we observe that using pre-training approach achieves the same reward performance as SPACE but improves reward slowly, and the pre-training approach has more cost constraint violations than SPACE. This implies that jointly using reinforcement learning and the supervision of the baseline policy achieve better reward and cost performance.

For d-CPO and d-PCPO, in the point and ant tasks we observe that both approaches have comparable or silently better reward and cost performance compared to SPACE. However, in the car-racing task we observe that d-CPO cannot improve the reward due to a slow update procedure for satisfying the cost constraint, whereas d-PCPO has a better reward performance. These observations imply that the projection steps in SPACE allow the learning agent to effectively and robustly learn from the baseline policy.

Comparison of SPACE under the KL-divergence and the 2-norm Projections (see Fig. 12).

Theorem 4.1 shows that under the KL-divergence and 2-norm projections, SPACE converges to different stationary points. To demonstrate the difference between these two projections, Fig. 12 shows the learning curves of the undiscounted constraint cost, the discounted reward, and the undiscounted divergence cost over policy updates for all tested algorithms and tasks. In the Mujoco tasks, we observe that SPACE under the KL-divergence projection achieves higher reward. For instance, in the point gather task the final reward is 25% higher under the same cost constraint satisfaction. In contrast, in the traffic management tasks, we observe that SPACE under the 2-norm projection achieves better cost constraint satisfaction. For instance, in the grid task SPACE under the 2-norm projection achieves a lower reward but more cost constraint satisfaction. In addition, in the bottleneck task SPACE under the 2-norm projection achieves more reward and cost constraint satisfaction. These observations imply that SPACE converges to different stationary points under two possible projections depending on tasks.

Initial h_D^0 (see Fig. 13). To understand the effect of the initial value of h_D^0 , we test SPACE with three different initial values: $h_D^0 = 1$, $h_D^0 = 5$, and $h_D^0 = 25$ in the ant circle and car-racing tasks. The learning curves of the undiscounted constraint cost, the discounted reward, and the undiscounted divergence cost over policy updates are shown for all tested algorithms and tasks in Fig. 13. In both tasks, we observe that the initial value of h_D^0 does not affect the reward and the cost performance significantly (*i.e.*, the mean of learning curves lies in roughly the same standard deviation over the initialization). In addition, the value of the divergence cost over three h_D^0 are similar throughout the training. These observations imply that the update scheme of h_D^k in SPACE is robust to the choice of the initial value of h_D^0 .

However, in the car-racing task we observe that the learning curves of using a smaller h_D^0 tend to have higher variances. For example, the standard deviation of $h_D^0 = 1$ in the reward plot is 6 times larger than the one with $h_D^0 = 25$. This implies that SPACE may have reward performance degradation when using a smaller initial value of h_D^0 . One possible reason is that when the distance between the learned and baseline policies is large, using a small value of h_D^0 results in an inaccurate projection (*i.e.*, due to approximation errors). This causes the policy to follow a zigzag path. We leave the improvement of this in future work.

E Human Policies

We now describe the procedure for collecting human demonstration data in the car-racing task. A player uses the right key, left key, up key and down key to control the direction, acceleration, and brake of the car. The human demonstration data contain the display of the game (*i.e.*, the observed state), the actions, and the reward. We collect 20 minutes of demonstration data. A human player is instructed to stay in the lane but does not know the cost constraint. This allows us to test whether SPACE can safely learn from the baseline policy which need not satisfy the cost constraints. We then use an off-policy algorithm (DDPG) trained on the demonstration data to get the baseline human policy. Since the learned baseline human policy does not interact with the environment, its reward performance cannot be better than the human performance. Fig. 14 shows the procedure.

Implementation Details of DDPG. We use DDPG as our off-policy algorithm. We use a convolutional neural network with two convolutional operators of size 24 and 12 followed by a dense layer of

size (32, 16) to represent a Gaussian policy. A Q function shares the same architecture of the policy. The learning rates of the policy and Q function are set to 10^{-4} and 10^{-3} , respectively.

F The Machine Learning Reproducibility Checklist (Version 1.2, Mar.27 2019)

For all models and algorithms presented, indicate if you include²:

- A clear description of the mathematical setting, algorithm, and/or model:
 - **Yes**, please see the problem formulation in Section 2, the update procedure for SPACE in Section 4, and the architecture of the policy in Section D.1.
- An analysis of the complexity (time, space, sample size) of any algorithm:
 - **Yes**, please see the implementation details in Section D.1.
- A link to a downloadable source code, with specification of all dependencies, including external libraries:
 - **Yes**, please see the implementation details in Section D.1.

For any theoretical claim, check if you include:

- A statement of the result:
 - **Yes**, please see Section 3 and Section 4.
- A clear explanation of any assumptions:
 - **Yes**, please see Section 3 and Section 4.
- A complete proof of the claim:
 - **Yes**, please see Section A, Section B, and Section C.

For all figures and tables that present empirical results, indicate if you include:

- A complete description of the data collection process, including sample size:
 - **Yes**, please see Section D.1 for the implementation details.
- A link to a downloadable version of the dataset or simulation environment:
 - **Yes**, please see Section D.1 for the simulation environment.
- An explanation of any data that were excluded, description of any pre-processing step:
 - **It's not applicable**. This is because that data comes from simulated environments.
- An explanation of how samples were allocated for training / validation / testing:
 - **It's not applicable**. The complete trajectories (*i.e.*, data) is used for training. There is no validation set. Testing is performed in the form of online learning approaches.
- The range of hyper-parameters considered, method to select the best hyper-parameter configuration, and specification of all hyper-parameters used to generate results:
 - **Yes**, we randomly select five random seeds, and please see Section D.1 for the implementation details.
- The exact number of evaluation runs:
 - **Yes**, please see Section D.1 for the implementation details.
- A description of how experiments were run:
 - **Yes**, please see Section D.1 for the implementation details.
- A clear definition of the specific measure or statistics used to report results:
 - **Yes**, please see Section 6.
- Clearly defined error bars:

²Here is a link to the list: <https://www.cs.mcgill.ca/~jpineau/ReproducibilityChecklist.pdf>.

- **Yes**, please see Section 6.
- A description of results with central tendency (*e.g.*, mean) variation (*e.g.*, stddev):
 - **Yes**, please see Section 6.
- A description of the computing infrastructure used:
 - **Yes**, please see Section D.1 for the implementation details.

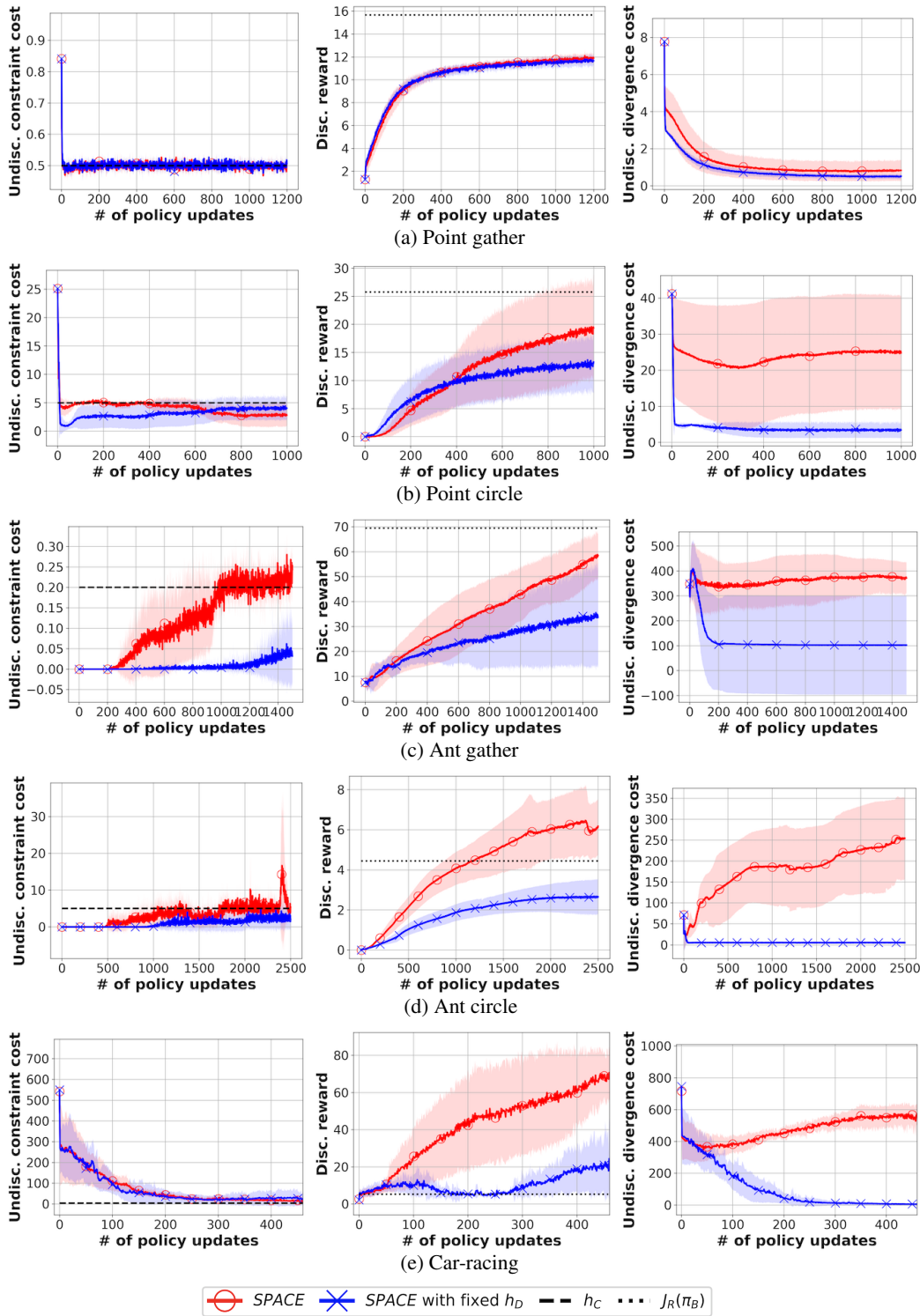


Figure 10: The undiscouted constraint cost, the discounted reward, and the undiscouted divergence cost over policy updates for the tested algorithms and tasks. The solid line is the mean and the shaded area is the standard deviation over 5 runs. SPACE with the dynamic h_D achieves higher reward. (Best viewed in color.)

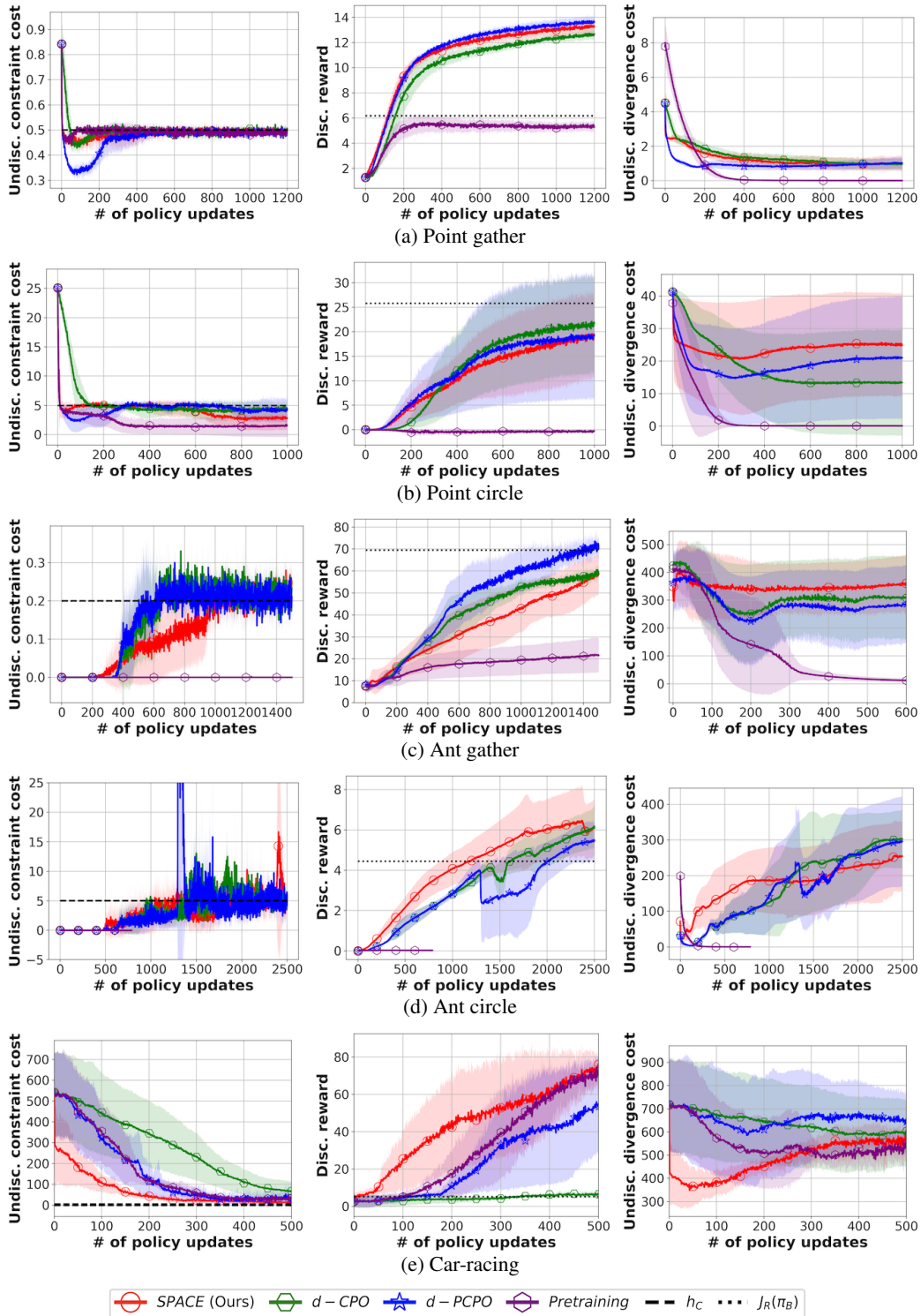


Figure 11: The undiscounted constraint cost, the discounted reward, and the undiscounted divergence cost over policy updates for the tested algorithms and tasks. The solid line is the mean and the shaded area is the standard deviation over 5 runs. SPACE outperforms d-CPO, d-PCPO and the pre-training approach in terms of the efficiency of the reward improvement and cost constraint satisfaction. (Best viewed in color.)

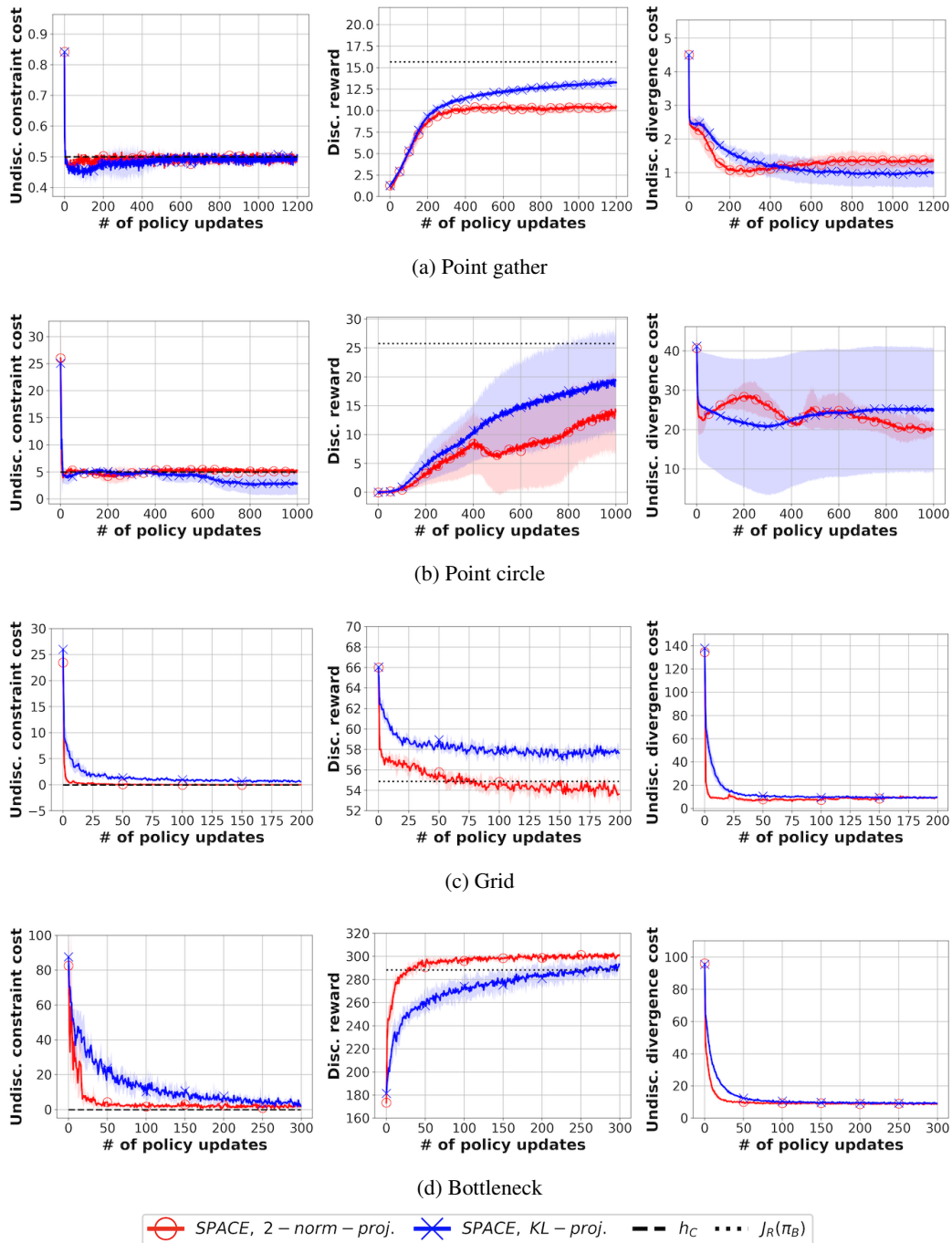


Figure 12: The undiscounted constraint cost, the discounted reward, and the undiscounted divergence cost over policy updates for the tested algorithms and tasks. The solid line is the mean and the shaded area is the standard deviation over 5 runs. SPACE converges to differently stationary points under two possible projections. (Best viewed in color.)

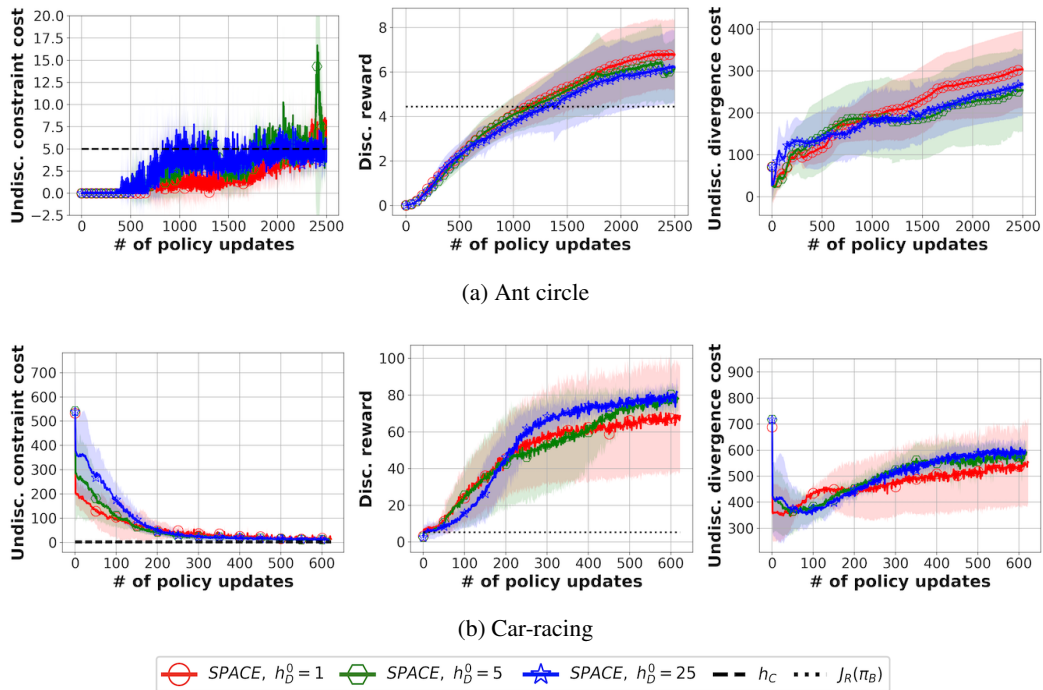


Figure 13: The undiscounted constraint cost, the discounted reward, and the undiscounted divergence cost over policy updates for the tested algorithms and tasks. The solid line is the mean and the shaded area is the standard deviation over 5 runs. We observe that the initial value of h_D^0 does not affect the reward and the cost performance significantly. (Best viewed in color.)

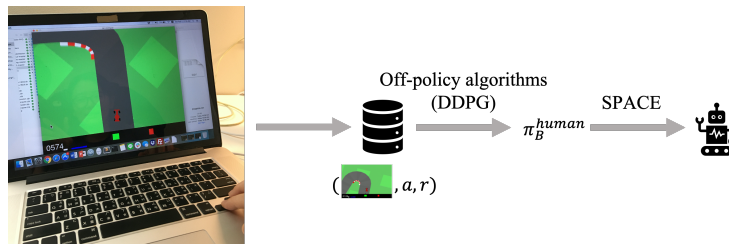


Figure 14: Procedure for getting a baseline human policy. We ask a human to play the car-racing game. He/She does not know the cost constraint. The trajectories (*i.e.*, display of the game, the action, and the reward) are then stored. A human policy is obtained by using an off-policy algorithm (DDPG) trained on the trajectories.